Modelling the effect of water harvesting structures on aeolian erosion in the Jordanian Badia

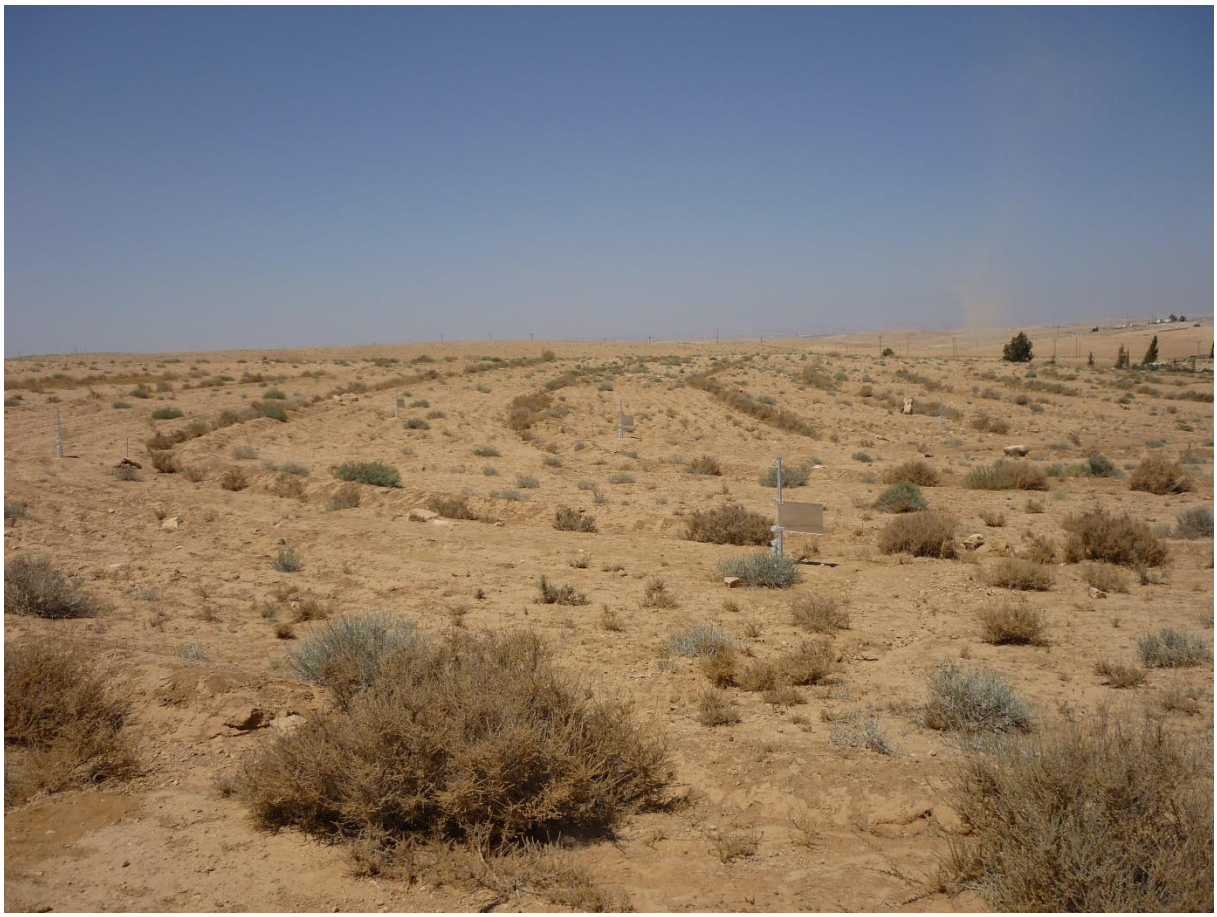

Anneloes Noordhoff

Universiteit Utrecht

ICARDA
Science for resilient livelihoods in dry areas

Modelling the effect of water harvesting structures on aeolian erosion in the Jordanian Badia

MSc Thesis

March - 2021

Anneloes Noordhoff

Student number: 4298837

E-mail: a.noordhoff@uu.nl

First supervisor: Geert Sterk

Second supervisor: Gerben Ruessink

MSc Programme: Earth Surface and Water

Faculty of Geosciences

Department of Physical Geography

Utrecht University

Preface

Here I present to you my Master thesis, presented in partial fulfilment of the Master programme Earth Surface and Water at Utrecht University, and written under extraordinary circumstances during the COVID-19 pandemic.
What initially started out as an exciting new project with a 3-month fieldwork period in Jordan, quickly changed into a work-from-home modelling study in the rainy Netherlands as the corona virus spread through the world. Nevertheless it has been an educational time, where I did not only learn a lot about wind erosion processes, but also about different model approaches and the relevance of field validation. Furthermore, cooperating with an international non-profit research organization, working with a high-end modelling system and creating my own model have been valuable experiences.
I want to thank Geert Sterk for the useful discussions, constructive criticism and overall excellent supervision. I also want to thank Mira Haddad and Stefan Strohmeier from ICARDA for their help in acquiring data, understanding the study area, and their positive feedback on many of my questions and proposals, and the people from AM&WFG of the University of Athens for their help in running the large scale model. I want to thank Tessa and Jessie for the helpful work sessions and mental support, and finally I want to thank my friends and family, for listening to my thoughts and worries and supporting me throughout this project.
Now, with this thesis coming to an end, the only thing left to do is visiting the Middle Eastern Desert, to see Jordan, Amman, the Badia and the water harvesting structures that have been both the backdrop and main character during this Master research.

I hope you will enjoy reading this thesis.

Anneloes Noordhoff
March 2021

Abstract

Arid and semi-arid regions are prone to wind erosion due to scarce rainfall and low vegetation cover. As transport of sediment by creep, saltation and suspension can lead to problems affecting the environment, climate and human health, methods to reduce aeolian erosion are continuously being researched. Water harvesting techniques have been applied in dry areas for a long time to reduce wind erosion, by increasing water storage and enhancing vegetation growth. In the Jordanian Badia (desert), Vallerani water harvesting structures have been implemented on an experimental site, but the effect on wind erosion reduction remains unclear. This study aimed to quantify the reduction in wind erosion by integrating a small scale cellular automaton model and a large scale model for Badia conditions with and without water harvesting structures. It also compared different transport equations to assess the uncertainty of the obtained values. The results are promising, as reductions in sediment transport of over 88% were obtained for the plot scale model. Outscaling to suitable areas is similarly promising, as the large scale model determined 60-100% reduction in dust concentration near the surface for areas where water harvesting structures are implemented on a regional scale. The coupling between the models can be optimized through the creation of new, specialized land cover classes with plot scale model values to be implemented in the large scale model. Improvements to the plot scale model can be made to include better vegetation spatial distribution, but field measurements are required to verify the use of model governing equations and validate the modelled sediment fluxes.

***Key words**:* wind erosion modelling, water harvesting structures, (semi-)arid regions, saltation, suspension

Table of Contents

Model parameters

Parameter	Value	Unit	Definition
$U(z)$		m s^{-1}	wind speed at height z
u_*		m s^{-1}	friction velocity
u_{*t}		m s^{-1}	threshold friction velocity
u_{*s}		m s^{-1}	surface friction velocity
k	0.4	-	Von Karman constant
z		m	height of air flow
z_0		m	aerodynamic surface roughness length
h		m	mean vegetation height
λ		-	vegetation density
n_{sh}		-	number of shrub roughness elements
n_g		-	number of grass roughness elements
b_{sh}		m	shrub sphere diameter
dx		m	cell size
R_d		m	distance between water harvesting rows
F		m^2	vegetation mean frontal area
η_{sh}		-	shrub porosity
h_a		m	grass height
w_g		m	grass width
S		m^2	surface area
γ		°	wind angle
ρ_s		kg m^{-3}	grain density
ρ_a		kg m^{-3}	air density
d		µm	mean particle size
D	250	µm	reference grain diameter
g	9.81	m s^{-2}	gravitational acceleration
a_1	0.0123	-	dimensionless parameter
a_2	3 x 10^{-4}	kg s^{-2}	dimensional parameter
τ_0		N m^{-2}	total shear stress or drag
τ_s		N m^{-2}	drag on ground surface
τ_r		N m^{-2}	drag on roughness elements (vegetation)
C_s		-	surface drag coefficient
C_r		-	vegetation (roughness) drag coefficient
β		-	drag ratio (C_r/C_s)
q		kg m^{-1} s^{-1}	suspension sediment flux
q_{max}		kg m^{-1} s^{-1}	maximum horizontal sediment flux
B	25	m	transport coefficient
dx		m	cell length
f_c		-	clay fraction of soil in %
q_{hs}		kg m^{-1} s^{-1}	horizontal mass flux
q_{vs}		kg m^{-2} s^{-1}	vertical mass flux
c_0	0.01-4.2	-	saltation constant
C_α	0.0006	-	dust emission constant
C_β		-	dust emission constant
p		Pa	soil plastic pressure
ReF		µm	Reynolds friction number
D_{opt}		µm	optimum particle size

List of figures

List of tables

1. Introduction

1.1. Background

Wind erosion is a global phenomenon that affects the environment, human health and climate (Dupont et al., 2014). The wind-driven movement of soil particles can cause soil degradation, such as loss of nutrients and reduced ability to retain moisture (Field et al., 2010), and can impact distant environments by for example altering ocean (bio)chemistry by deposition of nutrients (Mahowald et al., 2009). Near civilized areas it can have health implications such as respiratory problems due to particle inhalation and contribute to the spread of diseases (Chen et al., 2010; Goudie, 2014; Soleimani et al., 2020). Ultimately it affects the climate by changing atmospheric radiative properties, cloud formation and energy distribution (Spyrou et al., 2013).

Wind erosion can occur when forces that drive particle movement are larger than forces that resist particle movement. The momentum transfer from the atmosphere to the surface, also called shear stress or drag, is the main driver of erosion, while surface characteristics such as soil type, soil moisture and vegetation cover play a role in resisting removal (Shao, 2008). These forces are generally represented by the friction velocity, which characterizes the driving wind shear at the surface, and the threshold friction velocity, which is the minimum friction velocity required to initiate motion (Shao & Lu, 2000). Particle movement resulting from these forces can be described by three different mechanisms: creep, saltation and suspension (Figure 1). Creep is the sliding of relatively large particles (> 500 µm) across the surface, saltation is the bouncing movement of sand particles (100-500 µm) over the surface and suspension is the entrainment of dust particles (< 100 µm) into the atmosphere (Bagnold, 1941; Sterk, 2003). The mode of transport is not only dependent on particle size, but is also controlled by the (threshold) friction velocity.

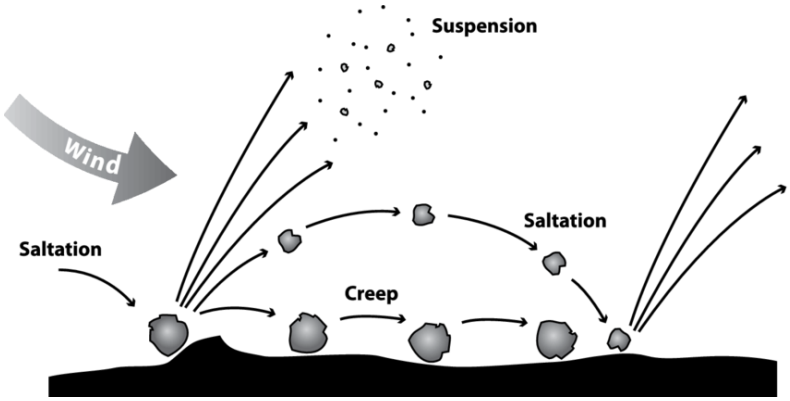

Figure 1. Modes of particle motion: creep, saltation and suspension (Presley & Tatarko, 2009).

Arid and semi-arid regions are prone to wind erosion, as large sand seas, low soil moisture and little to no surface cover create optimal conditions for aeolian erosion and transportation (Shao, 2008). Drylands cover about a third of the land on earth, of which 4% is extremely arid, 15% is arid and 14.6% is semi-arid (Cooke & Warren, 1973). Examples are the Sahara Desert in North Africa, the Patagonian Desert in South-America and the Middle Eastern Desert that spans from Saudi-Arabia and Yemen to Iraq and Jordan. Dust storms are frequently observed in these areas and are expected to increase in occurrence, as climate change leads to increased desertification and more extreme weather (IPCC, 2019). This will create major challenges for environmental managers and policy makers to keep wind erosion to a minimum.

Methods to reduce aeolian erosion are continuously being researched and implemented. An often-used measure to lower erosion rates is by (re)introducing vegetation. Grasses, shrubs and/or trees form obstacles on the surface, thereby absorbing momentum from the wind and reducing its

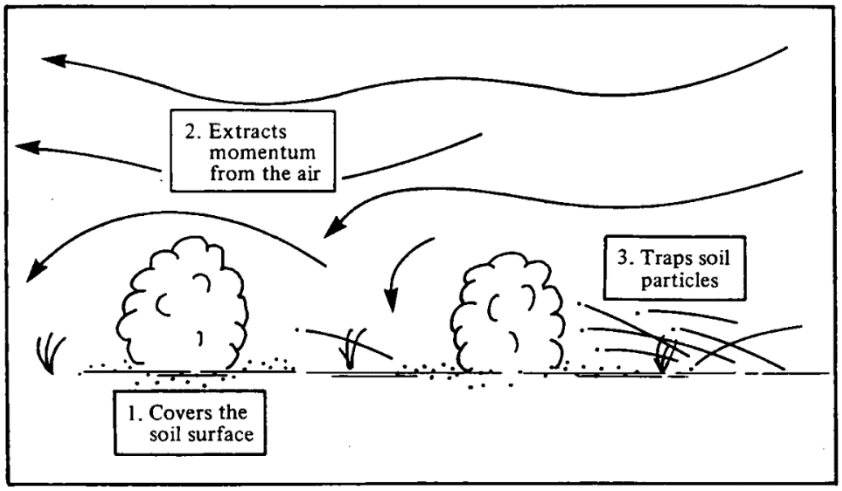

Figure 2. The effect of vegetation on sediment transport (Wolfe & Nickling, 1993).

erosive power (Figure 2). They also protect the soil with their cover and trap sediment already in transport (Fryrear & Skidmore, 1985; Wolfe & Nickling, 1993). However, in dry areas, growing vegetation can be challenging due to low moisture availability. To make optimal use of scarce rainfall, rainwater harvesting (WH) systems are increasingly being implemented. These systems effectively collect and store water, thus enhancing soil moisture and vegetation growth (Oweis, 2017). An example of such a WH system is the Vallerani system: a modified mechanized plow that makes trenches and ridges in the landscape that slow and stop surface runoff (Figure 3). Seeds and shrubs can be planted in the trenches where they can grow, providing protection for the soil and food for livestock (Ali et al., 2006).

Wind erosion research has been ongoing for decades and continuous progress is being made, but the physics of wind erosion is complex and many processes are still not fully understood. It involves many factors (atmospheric, soil and land-surface processes) that interact during erosion events, causing it to be highly variable in space and time. The complexity of aeolian erosion makes it difficult to accurately predict its occurrence and assess the effectiveness of mitigation measures. Efforts in modelling aeolian soil erosion have given insight into the driving forces and feedback systems and can indicate areas susceptible to wind erosion due to environmental conditions (wind speed and direction, soil type and state, surface morphology) (eg. Marticorena & Bergametti, 1995; Okin, 2008; Spyrou et al., 2010). It can furthermore assist in assessing the effectiveness of various measures (eg. Dupont et al., 2014; Mayaud & Webb, 2017; Okin & Gillette, 2001).

1.2. Problem definition

Vallerani water harvesting structures have been implemented and tested in the field on small scale plots, for example in the Jordanian Desert, also called 'Badia', and seem effective in collecting and storing water and enhancing vegetation growth (Ali et al., 2006; Yousef et al., 2018). However, the effect of these WH structures on wind speed and erosion reduction remains unknown. As the

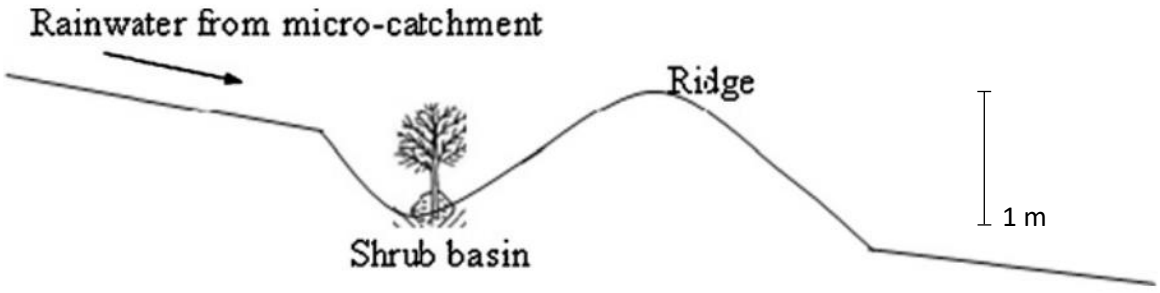

Figure 3. Vallerani water harvesting concept (Ali et al., 2010)

Badia is a place where dust production occurs frequently and where both nearby civilizations (for example people in the city of Amman) as well as distant environments can experience the negative effects of this, quantifying erosion reductions is an important process for the implementation of these measures.

Wind erosion is highly variable in space and time, especially with sparse vegetation present, and accurate representation of small scale processes is important in erosion modelling (Okin & Gillette, 2001). The relationships between atmospheric and land surface processes provided by wind-tunnel and field experiments are useful in evaluating small scale wind erosion (Bagnold, 1941; Dong et al., 2003; Shao et al., 1993; Sterk et al., 2012; Zingg, 1953), but the difficulty in assessing the larger effect of WH structures arises from the complexity of translating the plot scale effects of WH structures on creep, saltation and suspension to large (regional) scale dust production rates. In regional to global scale models, where grid size is generally too large to represent small scale processes, necessary values are averaged over relatively big distances, thereby losing the sub-grid heterogeneity of the surface that is crucial in many of these processes. The results from these models are then difficult to validate on a physical basis, and may over- or underestimate erosion compared to point measurements (Webb & McGowan, 2009). This study will therefore attempt to integrate a small and large scale wind erosion model, to improve large scale dust production simulations and quantify erosion reduction by Vallerani water harvesting structures in the Jordanian Badia.

1.3. Research question and objectives

The main research question of this study was: what is the effect of Vallerani water harvesting structures on wind erosion and dust production in the Jordanian Badia? To answer this question, the study attempted to develop a modelling approach that enables simulations of wind erosion and dust production in relation to Vallerani water harvesting structures. The objectives of this study were threefold:

1. to model the effect of Vallerani water harvesting structures on wind speed and saltation transport reductions at the plot scale;
2. to couple the field scale model with a large scale dust production model for simulation of saltation and suspension fluxes in the Badia environment;
3. to quantify reductions in wind erosion and dust production by using Vallerani water harvesting structures at large scale in the Badia.

2. Study Area

The study area is located in the Jordanian desert, locally called Badia (Figure 4). Jordan is a country in the Middle East and borders with Syria in the north, Saudi-Arabia and Iraq in the (south)east and Israel and Palestine in the west. It has an arid to semi-arid climate (Kottek et al., 2006), with hot summers and mild winters. Average temperatures fluctuate throughout the year from 10°C in winter to 24.5°C in summer, with extremes of -5°C to 46°C occurring occasionally (Al-Homoud et al., 1995). The annual precipitation ranges from over 600 mm in the western highlands to less than 100mm in large parts of the Badia. The precipitation in the Badia falls in sporadic but intense rainstorms and summers are very dry (Abu Sada et al., 2015). Wind direction and speed in the Badia vary with the seasons. The main wind direction during winter is west-southwest, caused by depressions along the Mediterranean region, while during summer the dominant wind has a northwest direction under the influence of the Indian Monsoon. Average wind speeds range from 4-8 m s^{-1}, with peaks during summer up to an average of 13 m s^{-1} (Al-Homoud et al., 1995).

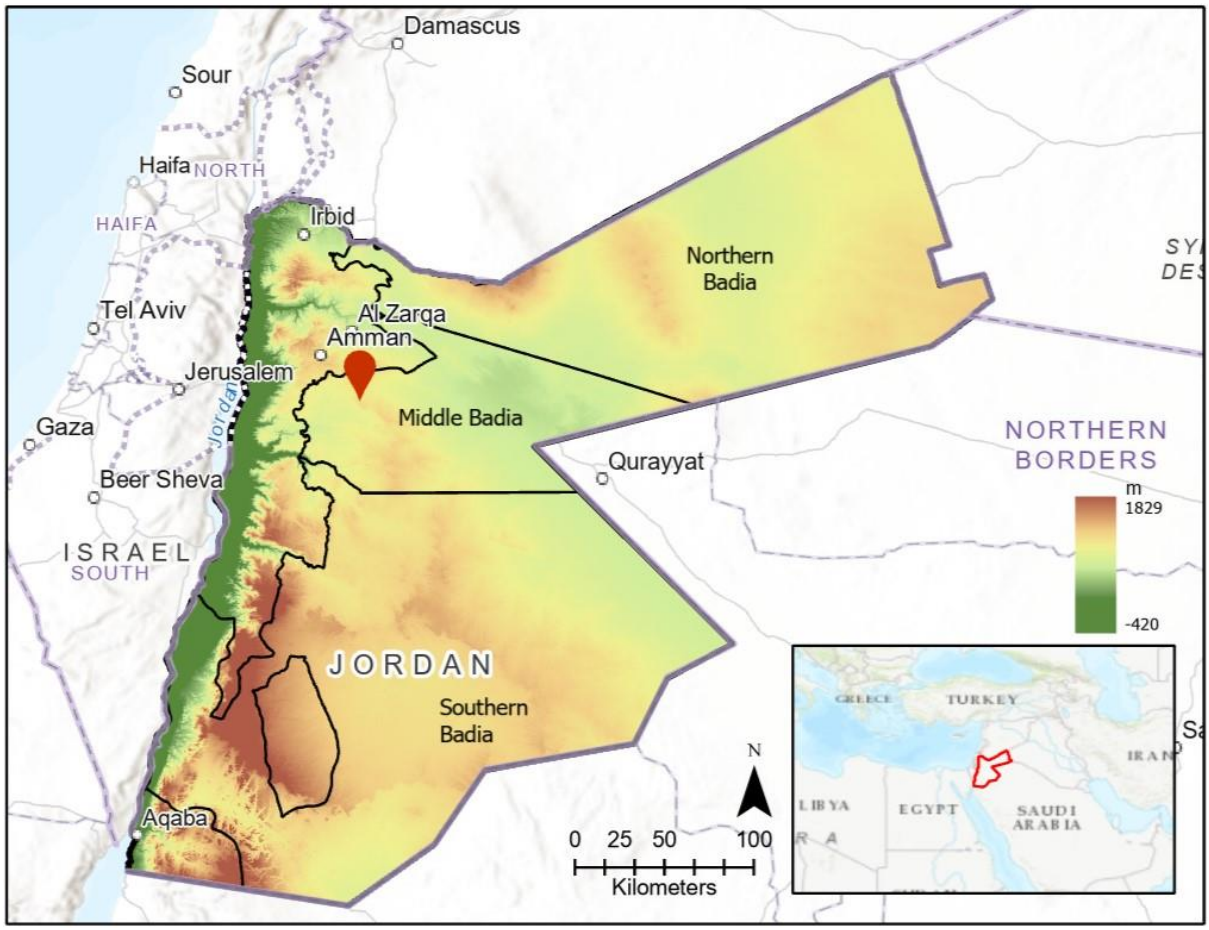

Figure 4. Map of Jordan showing elevation (from ASTER (2018)) and Badia regions. The red pin indicates the location of the study area Al Majidiyya.

Over 80% of the 90,000 km^2 of the country's land surface encompasses the desert, subdivided into the North Badia (35.7%), Middle Badia (13.3%) and South Badia (51%). The erratic and sparse nature of rainfall and high evaporation rates make this an area with little vegetation, mainly consisting of rangeland and pastures (Figure 5). The soils are high in silt and calcium carbonate, and consist mainly of silty loam to silty clay loam. The gentle to moderate slopes (2-20%), in combination with a soil prone to crusting, lead to low infiltration and high runoff rates. With a relatively flat topography and little surface cover, high wind speeds and gusts can develop. The natural vegetation in this region

Figure 5. The Middle Badia in Jordan near Amman (photo by: Mira Haddad, ICARDA).

consists mainly of shrubs (eg. Atriplex Halimus, Atriplex Leucoclada, Salsola Vermiculata) and grasses, creating harsh but somewhat liveable conditions (Karrou et al., 2011). The Badia is inhabited by Bedouin, semi-nomadic pastoralists that herd sheep, goats, cattle and camels. Although originally mobile year-round, increased demand for livestock feed has shifted their lifestyle to semi-intensive agriculture, mainly cultivating barley. The change from nomadic to semi-nomadic has strongly increased the pressure on the rangeland. Overgrazing and (inappropriate) land cultivation, in combination with a changing climate, play an important part in declining vegetation cover and increasing wind erosion (Al-Homoud et al., 1995; Karrou et al., 2011).

The use of WH structures to restore and conserve the land is thousands of years old (Oweis et al., 2001) and the vast, dry environment of the Jordanian Badia makes it an excellent place for water harvesting research (Ali et al., 2006; Gammoh & Oweis, 2011). The International Center for Agricultural Research in the Dry Areas (ICARDA) has set up the experimental site Al Majidiyya, about 40 km southeast of Amman, to investigate the possibilities and benefits of different water harvesting techniques. The creation of sustainable agricultural systems would allow exploration of implementation in other dry areas of West Asia and North Africa.

The Vallerani WH technique has been applied in Al Majidiyya in a small catchment of about 16 ha with water harvesting structures along the contour lines of the slopes (Figure 6), to assess its efficiency in capturing and utilizing surface runoff. The differences in vegetation cover between seasons can be seen clearly. On the long term, plant survival rates have been shown to be 40-70% higher when

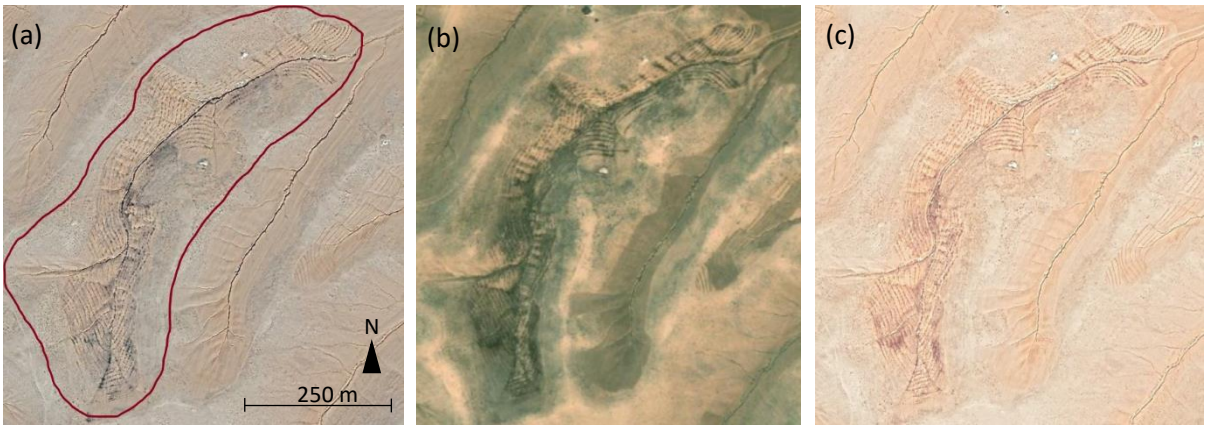

Figure 6. Catchment (circled in red) at research site Al Majidiyya in Jordan with Vallerani water harvesting structures in a) December 2018, b) June 2019 and c) December 2019 (images adapted from Google Earth Pro).

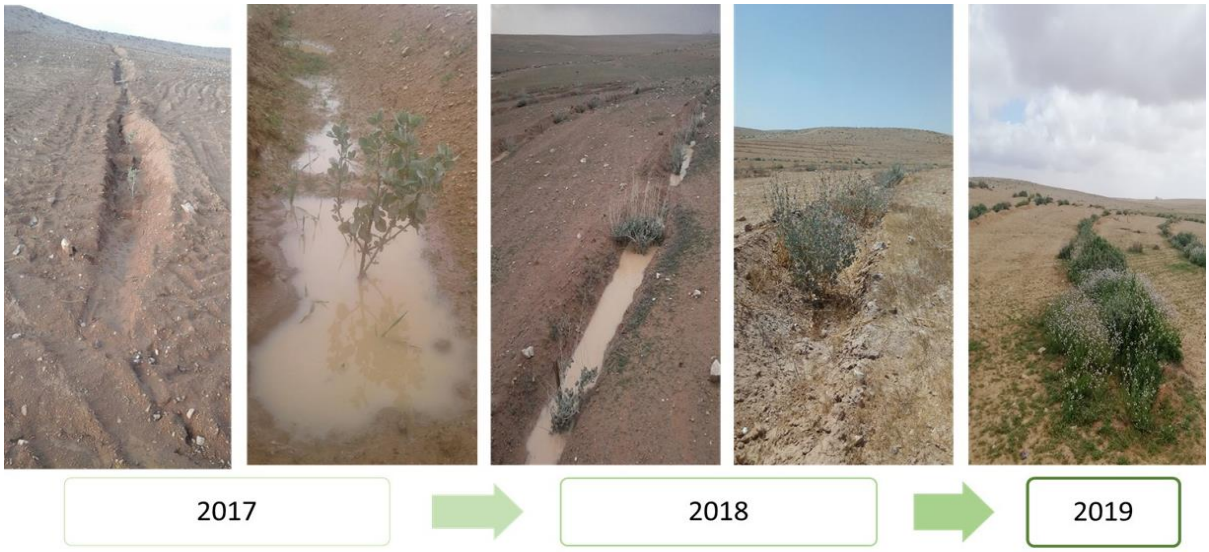

Figure 7. Development of vegetation in Vallerani water harvesting structures on ICARDA's Al Majidiyya research site in the Jordanian Badia (images by Mira Haddad, ICARDA).

seedlings are planted in WH structures such as those made using the Vallerani method (Ali & Yazar, 2007) and can thus be valuable in wind erosion reductions as well. Figure 7 shows that the development of vegetation has been promising over the years. Further details of the Vallerani structures and vegetation data at the research site Al Majidiyya are given in section 3.3.

3. Materials and Methods

To assess the wind erosion reduction by Vallerani water harvesting structures, first a cellular automaton model was used to simulate creep, saltation and suspension on the plot scale. The results of this model were then coupled with the RAMS-ICLAMS modelling system to simulate dust production on a larger scale. Model descriptions are provided below.

3.1. Model description

3.1.1. Cellular Automaton saltation model

A cellular automaton (CA) model is a type of model that is based on the interactions between cells. It is a spatially and temporally discrete computational system, consisting of a finite number of cells (in a grid), whose values are updated at each time step based on transition rules and relationships. Usually these transition rules involve the cell's own state and interactions between nearby cells, and can thus be seen as local positive or negative feedbacks (Favis-Mortlock, 2004). Although acting on a local scale, CA models have been able to simulate complex and self-organizing systems (eg. Vicari et al., 2007; Wang et al., 2006).

The cellular automaton saltation and suspension (CASS) model used in this study is based on a model developed by Smeets (2020) for aeolian transport simulations in the Aral Sea region. It is a 1D wind erosion model that calculates sediment transport (both creep + saltation and suspension) based on local atmospheric, soil and vegetation characteristics. Per time step, it calculates for each grid cell the variables needed to determine erosion and transport, including adjacent cells. For each time step it assumes a different wind velocity and updates the total erosion and transport in the grid accordingly, taking into account the previous time step. The wind direction is assumed be perpendicular to the water harvesting structures.

Friction velocity

The friction velocity (m s^{-1}) is calculated as (Wolfe & Nickling, 1993):

$$u_* = \frac{U(z) * \kappa}{\ln\left(\frac{z}{z_0}\right)} \qquad z \geq z_0 \tag{3.1}$$

where $U(z)$ is the mean horizontal wind speed (m s^{-1}) at height z (m), z_0 is the (aerodynamic) roughness length (m) and κ is the von Karman constant (-), which for the atmospheric boundary layer ranges between 0.35 and 0.4 and is generally set at 0.4. The roughness length is the theoretical height at which the wind speed becomes zero when extrapolated downward. On a smooth bare surface z_0 is small, but with roughness elements present, the absorption of momentum of the wind by these obstacles slows down the wind speed, which is reflected by an increase in z_0. This roughness length is calculated with:

$$z_0 = 0.5h\lambda \tag{3.2}$$

where h is the mean vegetation height (m) and λ is the vegetation density (-), given as:

$$\lambda = nF/S \tag{3.3}$$

where S is the ground area (m^2) occupied by n roughness elements (-), each with mean frontal area F (m^2) (Raupach, 1992; Wolfe & Nickling, 1993). The number of roughness elements is calculated by:

$$n = dx/R_d \tag{3.4}$$

where dx is the cell size and R_d is the distance between the rows.
The vegetation density is calculated for each roughness element type individually. In this model, the roughness elements can consist of shrubs and/or grasses. The shape of the shrubs is assumed to be a sphere, with a frontal area calculated as:

$$F_{sh} = \pi(\frac{1}{2}b_{sh})^2\eta_{sh} \tag{3.5}$$

where b_s is the diameter of the shrub and η_s is the porosity of the shrub. The grass frontal area is calculated as:

$$F_g = h_g w_g \gamma \tag{3.6}$$

where h_g is the height of the grass, w_g is the width of the individual grass blades and γ is the number of grass blades on 1 m^2. The total frontal density λ is the addition of the shrub frontal density and the grass frontal density.
The mean vegetation height h is given as:

$$h = (n_{sh} * b_{sh} + n_g * h_g)/\lambda \tag{3.7}$$

where n_{sh} and n_g are the number of shrubs and grasses over the specified ground surface. For grass, this indicates how many m^2 with grass are present in this area.
Because wind direction can vary, the model includes an option to set the wind angle. By default it is set to zero, but if it gets another value, the distance between the rows is updated by:

$$R_d = \frac{R_d}{\cos\left(\gamma * \frac{\pi}{180}\right)} \tag{3.8}$$

where γ is the wind angle in degrees.

Threshold friction velocity

The threshold friction velocity (m s^{-1}) for ideal conditions is calculated according to (Shao & Lu, 2000)

$$u_{*t} = \sqrt{a_1 \frac{\rho_s}{\rho_a} gd + \frac{a_2}{\rho_a d}} \tag{3.9}$$

where ρ_a is the air density (kg m^{-3}), ρ_s is the grain density (kg m^{-3}), d is the mean particle size (µm) and g is the gravitational acceleration (m s^{-2}), a_1 is a dimensionless parameter and a_2 is a dimensional parameter (kg s^{-2}). Shao & Lu (2000) determined a_1 to be 0.0123 and a_2 between 1.65 x 10^{-4} and 5 x 10^{-4} kg s^{-2}.

Drag partitioning

Drag partitioning is the distribution of total shear stress τ_0 (N m^{-2}) between the shear stress at the surface and the shear stress on the roughness elements. It can be calculated using the approach of Raupach (1992):

$$\tau_0 = \rho_a u_*^2 = \tau_r + \tau_s \quad (3.10)$$

where τ_r is the pressure drag on the vegetation (roughness elements) (N m^{-2}) and τ_s is the skin drag on the ground surface (N m^{-2}). In absence of vegetation or other roughness elements, τ_r = 0 and $\tau_0 = \tau_s$. τ_r and τ_s are calculated as follows:

$$\tau_r = \frac{\beta\lambda\tau_0}{1+\beta\lambda} \quad (3.11)$$

$$\tau_s = \frac{\tau_0}{1+\beta\lambda} \quad (3.12)$$

with the drag ratio β calculated as:

$$\beta = \frac{C_r}{C_s} \quad (3.13)$$

where C_s is the surface drag coefficient (-) and C_r is the vegetation (roughness) drag coefficient (-). C_s depends on the soil type and C_r is calculated as:

$$C_r = \frac{C_g n_g + C_{sh} n_{sh}}{n_g + n_{sh}} \quad (3.14)$$

where the subscripts g and sh represent grasses and shrubs. The friction velocity on the surface can then be written as:

$$u_{*s} = \sqrt{\tau_s/\rho_a} \quad (3.15)$$

For more detailed derivations of these equations the reader is referred to Raupach (1992).

Horizontal sediment flux: creep + saltation

If the friction velocity at the surface u_{*s} is larger than the threshold friction velocity u_{*t}, sediment transport can occur. However, many different equations exist that calculate the amount of creep and saltation (horizontal mass flux). Early sediment transport equations included only grain diameter and wind speed as variables governing the sediment flux, whereas later on also the threshold friction velocity became an essential variable. It is difficult to determine which equation is most suitable for any given situation, as they are all based on the same principle and vary purely in minor underlying assumptions, measurement uncertainties and consequently in the parameters that are used to account for local conditions. As soil characteristics such as texture and moisture can be highly variable in space, field research has shown that these parameters have a large range and they should ideally be determined empirically for locations other than those that they were originally proposed for (Shao, 2008; Sterk et al., 2012). The difference between sediment flux values from different equations can be as large as a factor 3 or more (Sarre, 1987) and may also be more inherent to the heterogeneity of the surface than to the chosen approach.

In the CASS model, the maximum amount of creep + saltation can be calculated with several approaches that use different variables, in order to assess the different results and decide which model performs best for the current research area. The five different options are:

1) Zingg (1953):

$$q_{max} = \frac{\rho_a}{g} u_{*s}^3 c_0 \left(\frac{d}{D}\right)^{\frac{3}{4}} \quad (3.16)$$

where q_{max} is the maximum horizontal sediment flux (kg m^{-1} s^{-1}), c_0 is a constant (-), d is the mean grain diameter (µm) and D is the reference grain diameter set at 250 (µm). Literature values for c_0 ranged from 0.01 to 0.83 and was in the model set to 0.3.

2) Kawamura (1964):

$$q_{max} = \frac{\rho_a}{g} u_{*s}^3 c_0 \left(1 - \frac{u_{*t}}{u_{*s}}\right)\left(1 + \frac{u_{*t}}{u_{*s}}\right)^2 \quad (3.17)$$

with c_0 ranging from 0.04-3.1 and in the model set to 0.1.

3) Maegley (1976):

$$q_{max} = \frac{\rho_a}{g} u_{*s}^3 c_0 \left(\frac{d}{D}\right)^{\frac{3}{4}} \left(1 - \frac{u_{*t}}{u_{*s}}\right)^{13.72} \quad (3.18)$$

with c_0 ranging from 0.024-0.467 and in the model set to 0.3.

4) Kind (1976):

$$q_{max} = \frac{\rho_a}{g} u_{*s}^3 c_0 \left(1 - \frac{u_{*t}}{u_{*s}}\right)^2 \quad (3.19)$$

with c_0 ranging from 0.072-0.534 and in the model set to 0.4.

5) Lettau & Lettau (1978):

$$q_{max} = \frac{\rho_a}{g} u_{*s}^2 c_0 \left(\frac{d}{D}\right)^{\frac{1}{2}} (u_{*s} - u_{*t}) \quad (3.20)$$

with c_0 ranging from 0.178-4.2 and in the model set to 0.6.

For this study, the optimal setting for c_0 for each equation was determined based on a combination of original values, values obtained by Sterk et al. (2012), and known field conditions. Kind (1976) showed that c_0 partly depends on particle diameter, having the highest values for sandy conditions. Sterk et al. (2012), who studied the same equations, obtained the highest values for Lettau & Lettau (1978) and the lowest for Kawamura (1964). As the soils in the study area consist of silty loam to silty clay loam, c_0 values were taken on the lower side of the ranges given. However, this empirical constant remains a large uncertainty in many modelling studies without field calibration, as values provided for the original equation have been shown to vary by several orders of magnitude (Sherman et al., 1998; Sterk et al., 2012).

The actual horizontal transport q_{hs_i} that occurs per cell i (= 1…n) is calculated with:

$$q_{hs_i} = q_{hs_{i-1}} + (q_{max} - q_{hs_{i-1}}) * (1 - e^{(-dx/B)}) \quad (3.21)$$

where dx is the length of the cell (m) and B is a coefficient (m) representing the rate of increase of total mass transport, in this model set to 25 (Sterk et al., 2012). The model assumes a non-erodible boundary at i = 1, indicating no incoming transport. If desired, the boundary condition can be adjusted to a specified value.

Vertical sediment flux: suspension

The amount of material brought into suspension q_{vs} is calculated from the horizontal flux q_{hs} and is calculated with 2 different dust schemes. Marticorena & Bergametti (1995) proposed:

$$q_{vs} = q_{hs} * 10^{0.134*f_c-6} \quad (3.22)$$

where f_c (%) is the clay fraction of the soil. Here, the vertical flux is directly proportional to the horizontal flux. Although this equation is generally used for soils with a clay content between 0 and 20%, and the clay content of the soil in the study area is higher (±30%), the approach is still used for its simplicity and easy implementation.

The second method used is the dust emission scheme by Lu & Shao (1999):

$$q_{vs} = q_{hs} * \frac{C_\alpha g f_c \rho_b}{2p}\left(0.24 + C_\beta u_* \sqrt{\frac{\rho_s}{p}}\right) \quad (3.23)$$

where p is the plastic pressure of the soil (Pa), ρ_b is the bulk density of the soil (kg m^{-3}), C_α is a constant set to 0.0006 (-) and C_β (-) is:

$$C_\beta = 0.137 * \frac{U(z)}{u_*} \quad (3.24)$$

The plastic pressure of the soil is difficult to determine, as it is dependent on many factors that need to be measured in the field for accurate estimation (a.o. soil moisture, crusting). For this study is was set to 30000 Pa, based on results from Lu & Shao (1999) and Shao (2004).

3.1.2. RAMS-ICLAMS modelling system

For the second part of this research, the CASS model results were coupled with the RAMS-ICLAMS modelling system to simulate large scale dust production. RAMS-ICLAMS is an atmospheric modelling system developed by the Atmospheric Modelling and Weather Forecasting Group (AM&WFG) at the University of Athens (Nickovic et al., 2001) and is based on the ETA/NCEP atmospheric model (Janjic, 1984; Mesinger et al., 1988). In the dust transport sub-model (SKIRON/Dust), the rates of dust production are calculated with the use of atmospheric and hydrological conditions resulting from the RAMS-ICLAMS model, and are controlled by soil type, vegetation cover, soil moisture content and surface atmospheric turbulence (Nickovic et al., 2001). The model runs over 2 domains: a large outer domain with a grid size of 200x200 m, and a smaller inner domain with a grid size of 100x100 m. For each grid cell it is determined whether it is a desert dust source, depending on soil and land cover at that point. The soil texture types are mapped into the horizontal model grid and average particle sizes and particle densities for clay, small silt, large silt, and sand fractions are estimated. Dust production is assumed to be initialized through saltation bombardment, the process when the impacts of the saltating grains eject smaller dust particles, which occurs when u_{*s} is greater than u_{*t} for a specific

particle size. The particle size dependent threshold friction velocity is determined with the use of the friction Reynolds number ReF (μm):

$$ReF = 1331 * D_{opt}^{1.56} + 0.38 \quad (3.25)$$

where D_{opt} is the optimum particle size (μm) that gives the lowest threshold friction velocity, assumed here to be ~60 μm (Spyrou et al., 2010). The threshold friction velocity is then calculated as:

$$u_{*t} = \begin{cases} \dfrac{0.129\left(\dfrac{\rho_s g D_{opt}}{\rho_a}\right)}{(1.928ReF^{0.092} - 1)^{0.5}} & 0.03 < ReF < 10 \\ 0.129\left(\dfrac{\rho_s g D_{opt}}{\rho_a}\right)(1 - 0.0858e^{-0.0617(ReF-10)} & ReF > 10 \end{cases} \quad (3.26)$$

The model also takes into account the dependence of the threshold friction velocity on soil moisture by relating it to the clay fraction according to Fécan et al. (1998). The horizontal mass flux (kg m^{-1} s^{-1}) is then calculated from the transport equation of White (1979), which is exactly similar to the one proposed by Kawamura (1964), but with a fixed value of c_0:

$$q_{hs} = c_0\left(1 - \frac{u_{*t}}{u_{*s}}\right)\left(1 + \frac{u_{*t}}{u_{*s}}\right)^2 \frac{\rho_a}{g} u_{*s}^3 \qquad c_0 = 2.61 \quad (3.27)$$

and the vertical mass flux (kg m^{-1} s^{-1}) is based on Marticorena & Bergametti (1995) (*3.22*).

The model has eight size bins incorporated with radii of 0.15, 0.25, 0.45, 0.78, 1.3, 2.2, 3.8, and 7.1 μm to accurately describe the mass distribution in long-term suspension. The dust production is further determined based on viscous/turbulent mixing, shear-free convection, diffusion and soil moisture, and includes a dry and wet deposition scheme as well as cloud scavenging (Spyrou et al., 2010). A more detailed description of the governing equation can be found in Nickovic et al. (2001) and Spyrou et al. (2010).

3.2. Approach

In this study, the CASS model was utilized to determine the parameters that can be used to optimize the RAMS-ICLAMS model. By using vegetation information of the water harvesting structures, as well as detailed soil properties of the area, horizontal and vertical fluxes were predicted on the plot scale. Also, by evaluating the different sediment transport equations, insight in the uncertainty range of these values was gained. Furthermore, the roughness length was examined closely, as this can vary for different scenarios and can be dominant in erosion and transport fluxes. Validation of the roughness length was done with linear regression of available high-resolution wind data.

From previous research into the potential for out scaling Vallerani water harvesting structures by Sarcinella (2020), the values of interest obtained from CASS for the plot scale were mapped for larger areas, to use as input in the RAMS-ICLAMS modelling system. The areas suitable for outscaling were based on the following static criteria:

- Cells with classes containing barren land/sparse vegetation, herbaceous vegetation and shrubland (all containing low vegetation cover), based on a land use/land cover map from ESA-CCI (2017);
- Cells with slopes up to 30%, selected from the digital elevation model (ASTER GDEM, 2018);

- Cells with average annual rainfall between 100 and 300mm, based on the CHIRPS[1] dataset;
- Cells with a soil depth of more than 50cm, based on ISRIC[2] data;
- Cells with a soil sand content of less than 50%, based on ISRIC data;
- Cells with a soil clay content of less than 50%, based on ISRIC data
- Cells with a stone content of less than 20%, based on ISRIC data.

The coupling of the two models was done by assigning an appropriate land cover class to the suitable areas for outscaling. The RAMS-ICLAMS model was run for the current situation, as well as for potential future scenarios that include large areas with Vallerani WH structures. Model performances can be validated in several ways, for example with satellite imagery as shown in Figure 8 for a large dust storm that passed over Jordan, or with available site measurements. In this study, MODIS imagery was used to compare modelled spatial dust distribution with real dust distribution, and dust concentrations (PM_{10} measurements) were compared to modelled fluxes. Finally, the reduction in dust production for both models were compared, to link the small scale effects of water harvesting structures to the large scale effects.

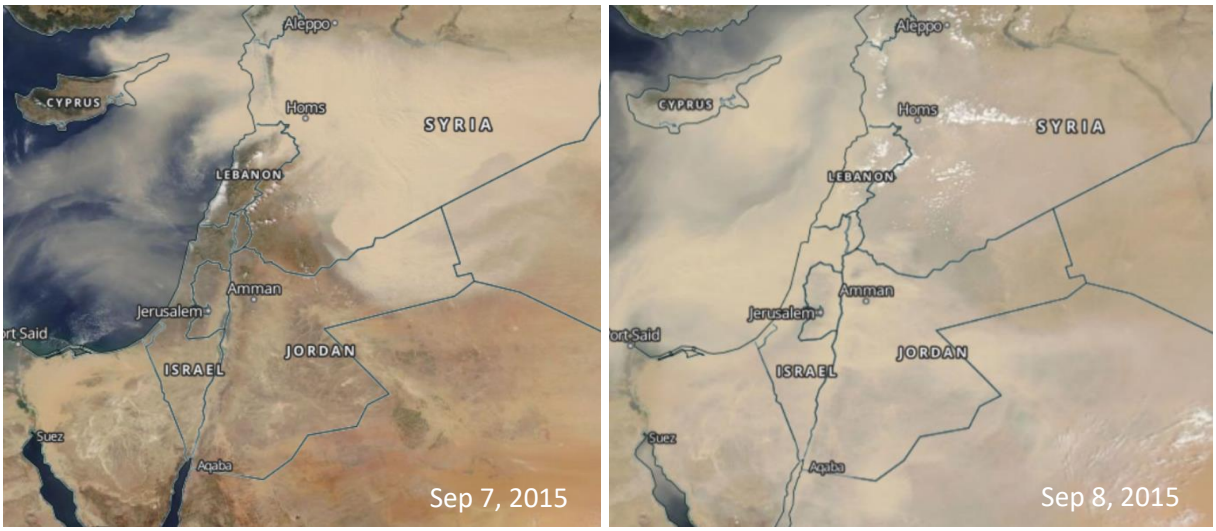

Figure 8. Dust storm over Jordan in September 2015. (MODIS imagery retrieved from https://worldview.earthdata.nasa.gov/)

3.3. Input data for modelling

CASS model

Required input for the CASS model was acquired from ICARDA, who provided detailed soil characteristics and field measurements of vegetation from field campaigns in among others 2011, 2019 and on request (Table 1). Vegetation porosity for different stages of the Vallerani WH structures (to account for differences in plant life cycles) was determined from images taken in the field, as well as the vegetation height and breadth. The spatial distribution of the vegetation is very regular due to the Vallerani structures: the rows are spaced 5-9 m apart, with seedlings planted every 1.5-2 m in the pits, on a plot of about 25 ha, resulting in at least 556 shrubs ha^{-1}. Figure 9 shows the set-up of the model grid for the different conditions used, with values from Table 1. 1 cell of 20m contained either bare soil, 3 rows of shrubs and/or 3 rows of grasses. For each cell of 20 m the average vegetation frontal densities (λ) and heights (h) were calculated based on these grids. The model runs for 12 cells

[1] Climate Hazards group Infrared Precipitation with Stations: http://climateengine.org/

[2] International Soil Reference and Information Centre: https://data.isric.org/geonetwork/srv/eng/catalog.search#/home

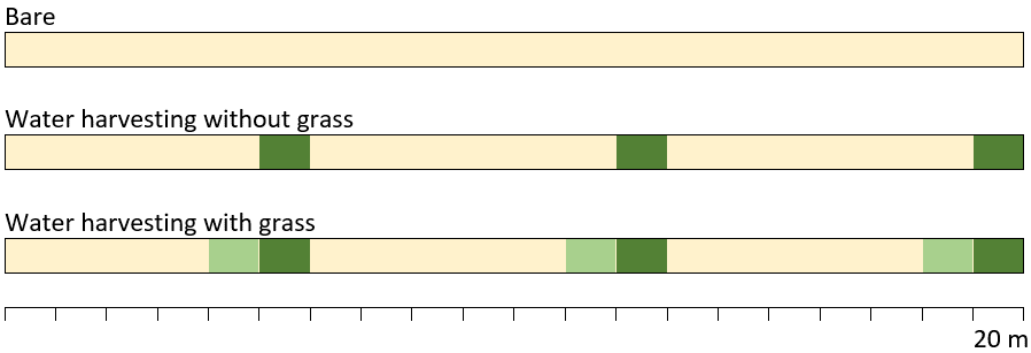

Figure 9. Representation of 1 cell of 20 m of different vegetation conditions used in CASS model. Average values of vegetation height and frontal densities are based on these representations.

with a total length of 240 m. It can also take into account different wind direction angles, making the spacing between the rows larger with increased angles.

The soil particle density was assumed to be 2.65 g cm^{-3} and the bulk density was measured at 1.35 g cm^{-3} (Akimoto, 2021). The average clay content ranged from 15-40% and was in the model set to 30% (Akimoto, 2021). The average grain diameter was 50 µm and the plastic pressure was set to 30000 Pa (Shao, 2004) (Table 1).

Hourly wind speed and direction data was acquired from ArabiaWeather for the station at Queen Alia International Airport, which is located about 13 km west of the research site Al Majidiyya. From this station, also other relevant meteorological data was available. This data was complemented with 5-minute wind speed and direction data from the Jordan Meteorological Department for the months October 2018 and March 2020. These months were chosen because of known dust storms that occurred on October 25, 2018 and March 12, 2020, based on local media reports and visibility information from the wind datasets. Furthermore, 1-minute wind speed and direction measurements for different environmental conditions were available from a field campaign in the summer of 2011. During this campaign, wind speeds were measured under three different conditions: natural, barley and Vallerani water harvesting (Figure 10) (Duijts, 2012). The availability of different datasets was used to validate model input and predictions.

RAMS-ICLAMS model

Required soil characteristics such as soil texture, bulk density, porosity, available water capacity and other soil physical properties were derived from the 30" Soil Texture Database, which is based on the U.S. Department of Agriculture's State Soil Geographic Database. This database includes all soil parameters that were needed for both the RAMS-ICLAMS atmospheric model and the SKIRON/Dust submodel (Spyrou et al., 2010).

Table 1. Vegetation and soil characteristics Al Majidiyya research site

Proporty	Unit	Shrub	Grass	Soil
Breadth	m	0.7	-	
Height	m	0.7	0.15	
Porosity	-	0.3	-	
Drag coefficient	-	0.2	0.1	0.003
Grain diameter	µm			50
Grain density	kg m^{-3}			2650
Bulk density	kg m^{-3}			1350
Clay content	%			30
Plastic pressure	Pa			30000

Figure 10. Image of wind speed measurements locations in Al Majidiyya, Jordan in 2011 with different vegetation settings: a) natural, b) barley (ridges parallel to wind directions) and c) water harvesting (images by Duijts (2012)).

Meteorological data for initial and boundary conditions were acquired from European Centre for Medium-Range Weather Forecasts (ECMWF) and National Oceanic and Atmospheric Administration (NOAA). The ESA-CCI land use/land cover map was used to determine vegetation cover for both the current situation and the scenario with large areas of water harvesting structures. For the WH scenario, the suitable areas for outscaling were determined as described in section 3.2 and shown in Figure 11. The new class was chosen as 'Wooded grassland', based on the closest correspondence between the parameters of this land cover class and known WH field characteristics. The updated ESA-CCI map was then used as input in the model to calculate surface variables.

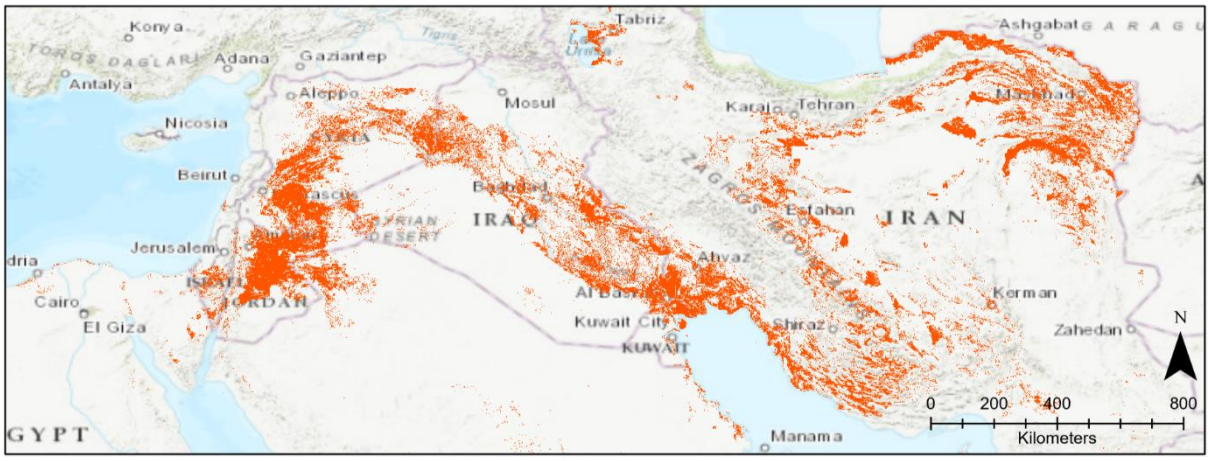

Figure 11. Map of areas suitable for outscaling Vallerani water harvesting structures in the Middle East (shown in orange), as used in the large scale model. Areas are based on selected criteria as outlined in section 3.2.

4. Results

4.1. Model input

4.1.1. Optical porosity

Field pictures were taken from several shrubs against a white background. To determine the optical porosity, these were converted to 8-bit black and white images with a digital image processing tool. Contouring was done by hand, based on expert opinion (Figure 12). The black and white threshold was set to 168 (pixel value cut-off) to ensure continuous classification.

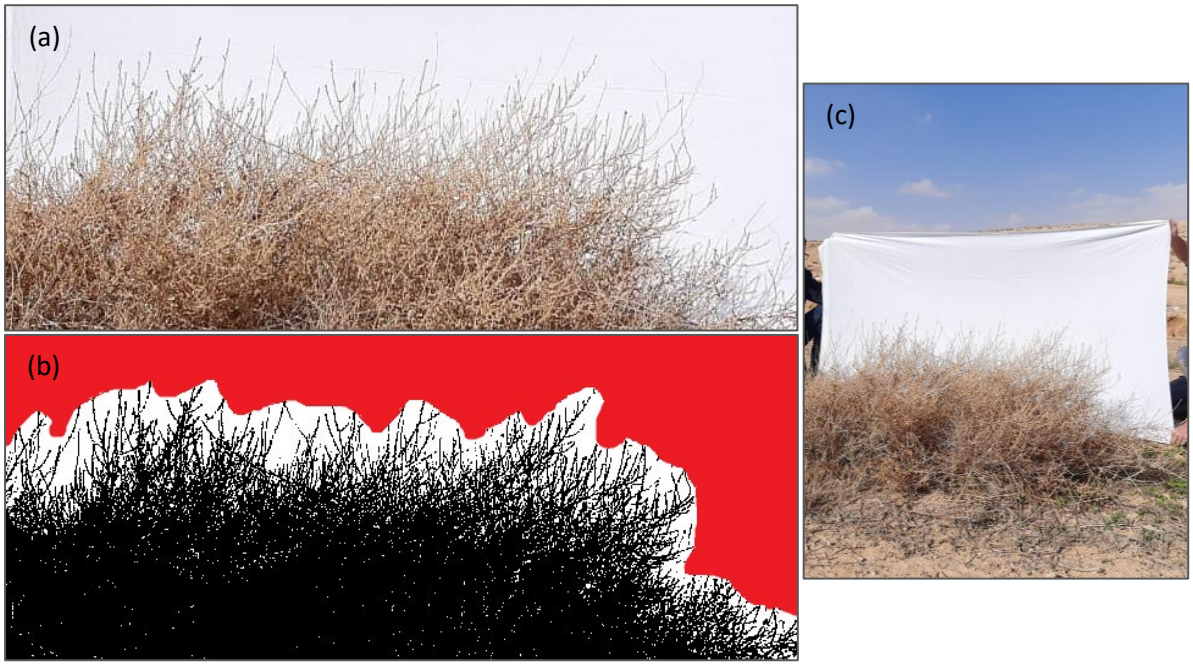

Figure 12. Optical porosity measurements for Salsola Vermiculata: (a) Shrub, (b) black and white analysis, (c) original field picture.

Table 2. Optical porosity measurements

Shrub	Black + white pixels	Black pixels	Porosity %
Salsola Vermiculata	114766	83760	**27.02**
Atriplex	147990	89218	**39.71**

The porosity was determined for two different plants, with an average of 33% (Table 2). Knowledge of additional shrub vegetation in the area with slight lower porosity led to the adoption of an average porosity value of 30% for all shrub vegetation. It should be noted that optical porosity is generally an underestimation of volumetric porosity, which is a better physical representation of how the wind interacts with the plant (Grant & Nickling, 1998), but such advanced measurements were outside the scope of this study.

4.1.2. Wind data validation

The hourly wind speed data from ArabiaWeather was supplemented with 5-minute data from the Jordan Meteorological Department. Comparison of the 2 datasets shows good agreement between original 5-minute measurements and the hourly measurements for the overlapping periods,

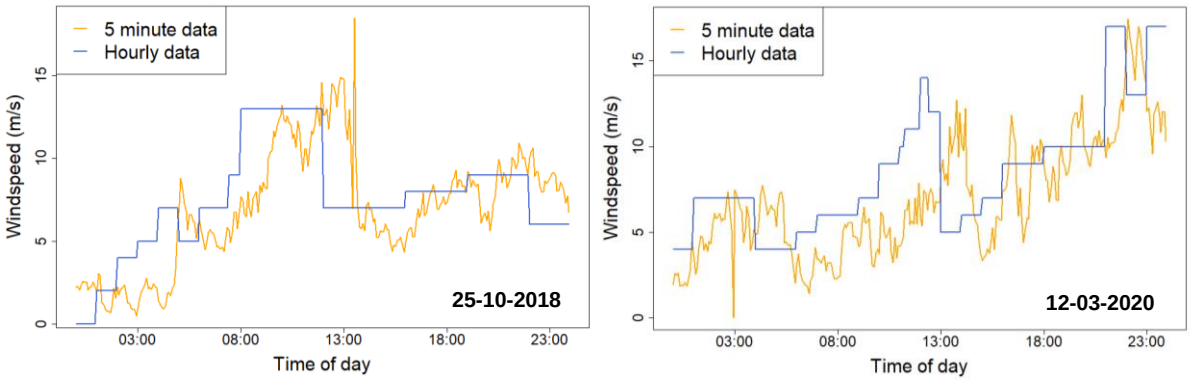

Figure 13. Comparison of 2 wind datasets (5-minute wind speed data from Jordan Meteorological Department and hourly wind speed data from ArabiaWeather, both measured at Queen Alia International Airport, Amman, Jordan at 10m height) for 25 October 2018 (left) and 12 March 2012 (right).

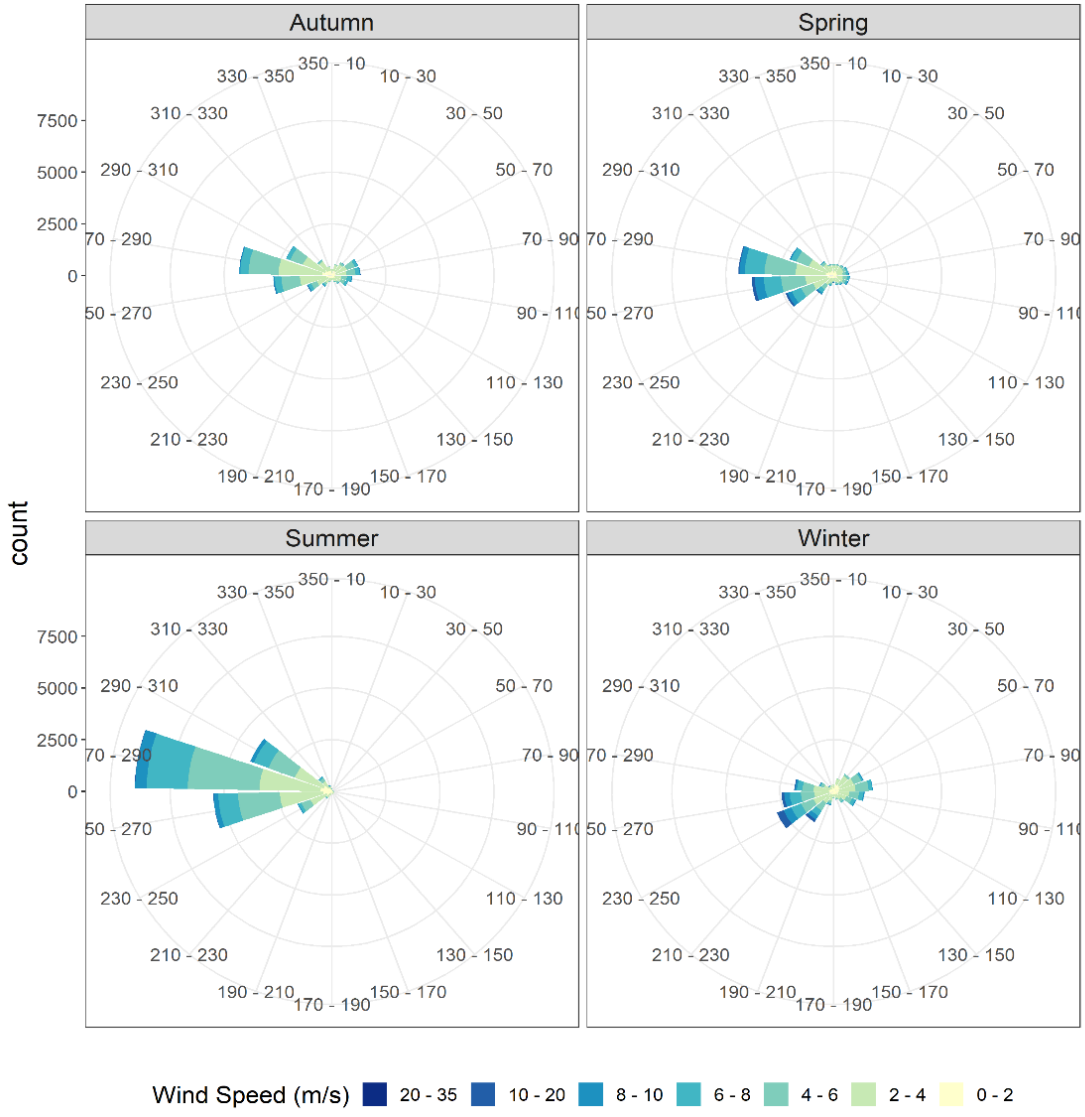

Figure 14. Wind roses (direction and speed) for spring (MAM), summer (JJA), autumn (SON) and winter (DJF), measured at Queen Alia International Airport, Amman, Jordan for 2010-2020.

with graphs of the two known dust storm days shown in Figure 13. This is promising for event simulations in months where 5-minute measurements are not available (either due to cost- or measurement restrictions), although it must be noted that extreme values are possibly diminished.

Wind direction and speed during the year were analysed. Direction is important for the roughness the wind encounters on the surface, especially with line structures like crop rows and water harvesting. Figure 14 shows that the main wind direction around the study area throughout the year is west, which is especially dominant during summer months. It is also clear that the highest wind speeds occur in winter and spring months (dark blue). These are important considerations in relation to vegetation stages and wind erosion.

4.1.3. Aerodynamic roughness length

The model calculates the aerodynamic roughness length (z_0) based on vegetation frontal area index and given vegetation height (*3.2*). The mean frontal indices (λ) for bare, WH without grass and WH with grass conditions were calculated at 0, 0.07 and 0.5, respectively, and vegetation height (h) is given in Table 1. As z_0 is an important variable in erosion studies in sparsely vegetated environments, it has been validated with wind speeds that were measured locally during the summer of 2011, for different settings of vegetation (natural, barley and Vallerani water harvesting structures, Figure 10) (Duijts, 2012). The calculated values from the field data show that in the water harvesting area the roughness length is the highest (0.0049 m) and natural vegetation slightly lower (0.0013 m), while barley conditions result in the lowest z_0 (0.0005 m). It should be noted that at the time of measuring the wind direction was parallel to the barley ridges, making the wind experience a much smoother surface as opposed to conditions where the wind direction is perpendicular to the ridges.

Because barley conditions were not modelled, only natural and water harvesting conditions have a modelled roughness length value. These values correspond closely to the values from the field: 0.001 m for natural conditions and 0.0052 m for water harvesting without grass conditions. The agreement of these values indicate good set up for this model component. Water harvesting with grass had a value of 0.03 m, but since there was no grass present during the field measurements, these values cannot be compared.

4.2. Horizontal flux

4.2.1. Transport equations

The five horizontal sediment transport equations (*3.16-3.20*) were used to calculate saltation and creep transport along the 240 m strip for three scenarios: bare soil, WH with grass and WH without grass (Figure 9). The simulations of WH with grass are more complex and uncertain, and therefore more difficult to interpret (as will be discussed in Chapter 5). Therefore, to keep this report concise, only results of the bare soil and WH without grass scenarios are shown here, as they are the most relevant in this research. However, all model results can be found in Appendix A. For visualization of the results, the third highest wind speed of the day was taken (as indicated in the figures), to exclude extreme results from possible measurement errors. The results shown here are for October 25, 2018; a day with high wind speeds (up to 18 m s^{-1}) and high dust concentration in the air. The modelled mass flux profiles are shown in Figure 15. The end-of-plot fluxes vary between 2.5 g m^{-1} s^{-1} to 10 g m^{-1} s^{-1} for the various transport equations. Based on the extremely high values that were obtained, the equation of Kind (1976) (*3.19*) was deemed unsuitable for the modelled conditions and was not used in further analysis. Figure 16 shows for the last cell of the modelled grid the total horizontal mass flux over time (cumulative) for both bare and water harvesting conditions. It shows that the four remaining equations perform quite similar up to a certain wind speed and under different vegetation settings. The equation of Lettau & Lettau (1978) (*3.20*) reacts more strongly to an increase in wind speed, possibly due to the dependence on u_{*s}^2 as opposed to u_{*s}^3 in the other equations. Zingg (1953) (*3.16*)

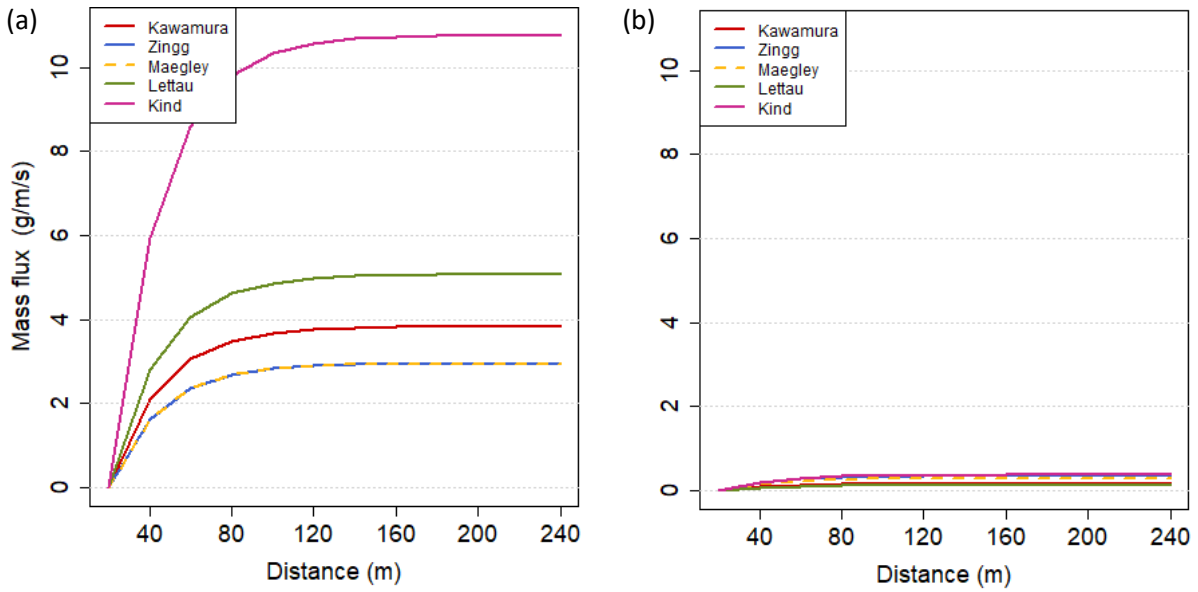

Figure 15. Horizontal mass flux at the research site of all transport equations for a) bare conditions and b) water harvesting without grass conditions. Modelled for selected wind speed (14.89 m s^{-1} at 10m height) at 25-10-2018.

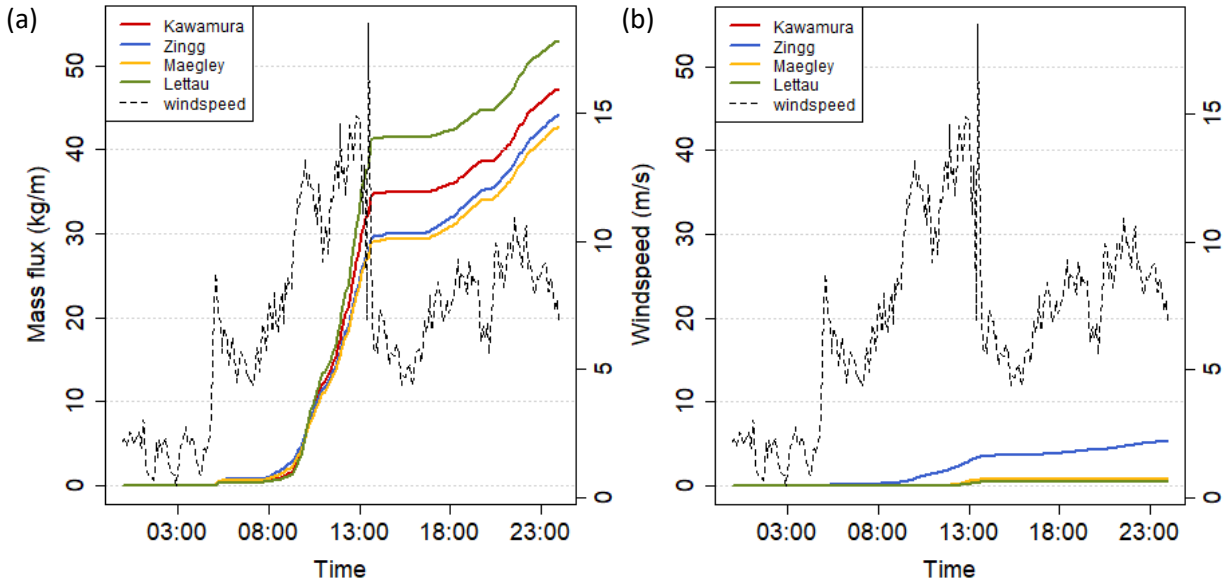

Figure 16. Cumulative horizontal mass flux in last cell of the plot at the research site for selected transport equations for a) bare conditions and b) water harvesting without grass conditions over 24 hours on 25-10-2018.

appears to be more strongly influenced by vegetation, possibly due to the lack of dependence on the relation between the friction velocity and the threshold friction velocity (which is altered with vegetation). For clarity, one transport equation was chosen to further visualize results. As the equation of Lettau & Lettau (1978) (*3.20*) also gives high results and the approach of Zingg (1953) (*3.16*) has a stronger vegetation dependency, the equation of Kawamura (1964) (*3.17*) was chosen for the remainder of this paper, also because this equation is often used in combination with vertical dust flux calculations (Kok et al., 2012) and has been shown to be relatively reliable in determining transport dynamics during erosion events (Sterk et al., 2012).

From Figures 15 and 16 it is clear that under water harvesting conditions the horizontal mass flux values are much lower than under bare conditions, for all transport equations considered. Figure 15 shows that from the non-erodible boundary at x=0, the horizontal mass flux increases towards a maximum determined by environmental conditions and transport equations, reaching it after about 200m. The cumulative horizontal mass flux over time in Figure 16 shows that after 24 hours over a

distance of 240 m about 50 kg m^{-1} of material has been transported. This corresponds to a soil loss of 0.15 mm in 24 hours (1.97 ton ha^{-1}), although deposition is not accounted for in this number. Under water harvesting conditions these values have been reduced by 88.0% (Zingg) to 99.4% (Lettau & Lettau) for all transport equations, giving a soil loss of 0.002-0.16 mm in 24 hours.

4.2.2. Mass flux, erosion and deposition

Figure 17 shows the mass flux of creep and saltation over time at the last cell of the plot on October 25, 2018. The Kawamura transport equation was used for both a bare plot (a) and a plot with Vallerani structures (b). The graphs follow, as expected, the wind speed curve. When mass flux values are 0, the wind friction velocity u_{*s} is below the threshold friction velocity u_{*t}, so no movement is initiated. When water harvesting structures are present, the friction velocity at the bare surface is lower due to shear stress partitioning, resulting in less transport (92%).

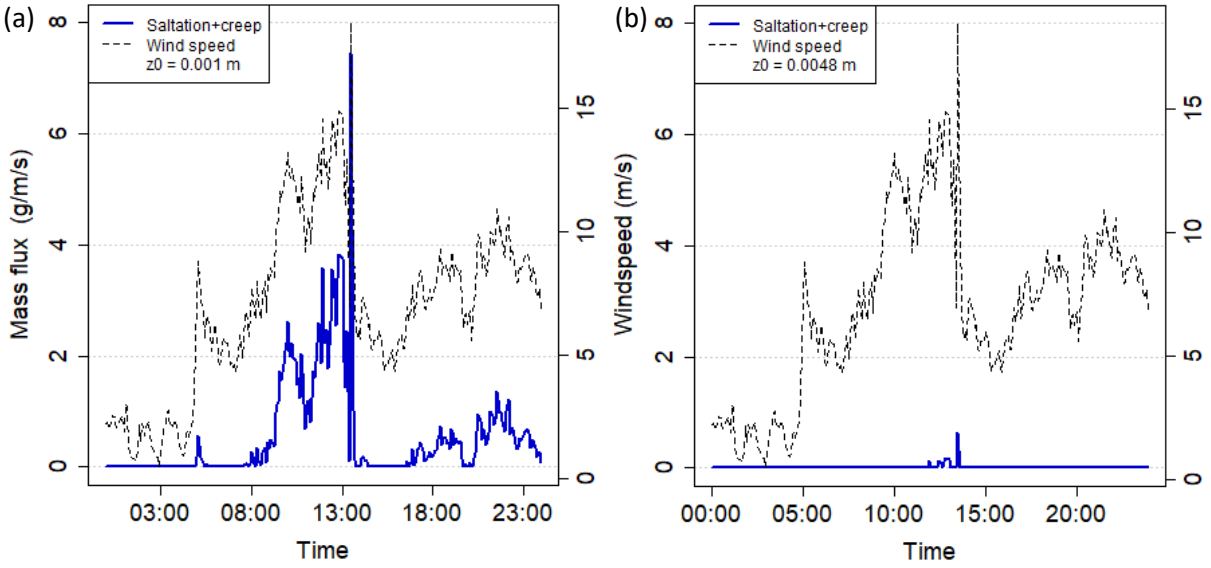

Figure 17. Horizontal mass flux in last cell of the plot at the research site for Kawamura transport equations for a) bare conditions and b) water harvesting without grass conditions over 24 hours on 25-10-2018.

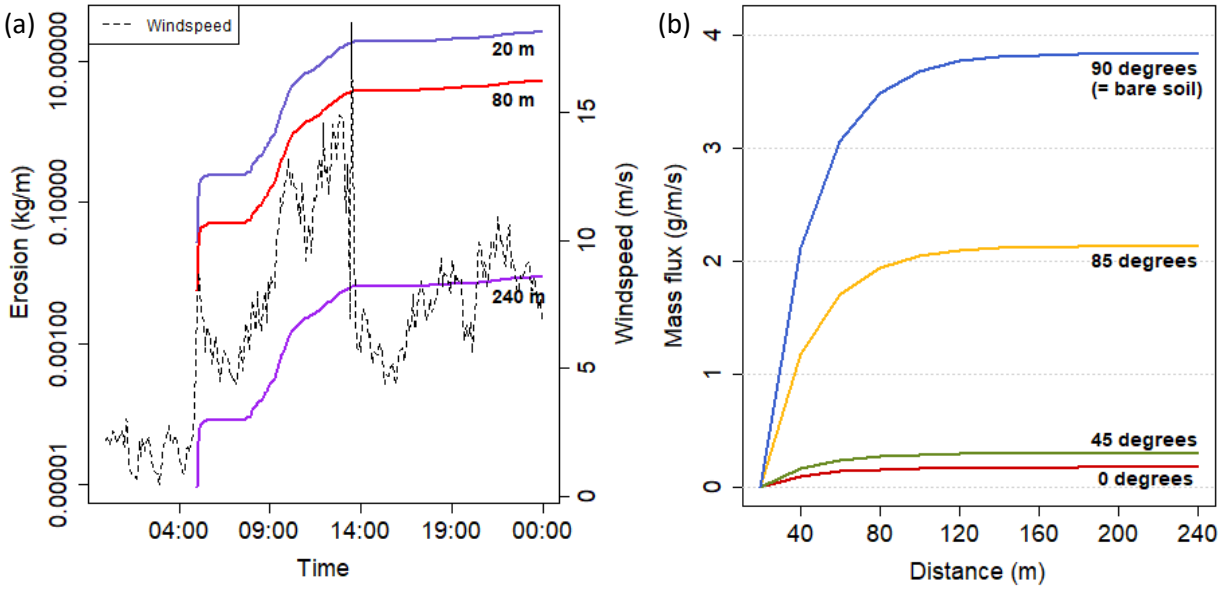

Figure 18. a) Spatial variation in erosion for 3 different cells. b) Horizontal mass flux under water harvesting conditions at the research site for the Kawamura transport equation under different wind angles.

The spatial variation in net erosion is displayed in Figure 18a for cells at 20, 80 and 240 m. As can be expected (from looking at the development of the mass flux in Figure 15) the erosion is highest in the cells closest to the non-erodible boundary and become almost zero in the cell at 240 m. Here, the carrying capacity of the wind has been reached and the amount of material coming in from upwind cells is practically equal to the amount of material leaving the plot. The same pattern occurs with water harvesting structures (not shown), but then about 88-99% reduced. As the model uses average vegetation values per cell, the true pattern for water harvesting scenarios is likely to be different, as further discussed in Chapter 5.

Figure 18b shows the variation in transport with varying wind angles. The main model results are assuming wind coming perpendicular onto the water harvesting rows, but as the rows are following contour lines (Figure 10c) and wind can come from various directions (Figure 14), transport can vary as well. With the wind blowing at an angle, the roughness decreases, as the distance between the water harvesting rows increases relative to the wind direction. It shows that small angles don't have a large influence on the total horizontal flux, but the larger the angle gets, the more erosion will occur.

4.3. Vertical flux

The vertical dust flux is directly related to the horizontal saltation and creep flux and is dependent on the clay fraction of the soil. Over distance, it shows the same development towards a maximum value (Figure 19). Over time, again a similar pattern as the horizontal flux is modelled, which is clearly related to wind speed (Figure 20). The dust scheme from Marticorena & Bergametti (1995) (*3.22*) gives a vertical flux about 3 times larger than the scheme from Lu & Shao (1999) (*3.23*). Under water harvesting conditions the flux is strongly reduced due to the decreased horizontal flux.

The cumulative suspension at the end of the plot over 24 hours (Figure 21) gives an indication of how much dust accumulates in the air. It shows the same patterns as the cumulative horizontal flux (Figure 16), although the mechanisms are different, as saltating particles get eroded and deposited (they are airborne over only short distances), while suspended particles remain in the air longer. The total of 500 g m^{-2} over 24 hours indicates an average vertical flux of 24 µg m^{-2} s^{-1}, although this of course varies over time with varying wind speeds.

The production of dust is much lower when water harvesting structures are present, indicating a lower dust concentration in the air. The total reduction is similar to what is shown in previous graphs: over 95% lower values are found for both dust schemes (Figure 19b) and the vertical average vertical flux is reduced to about 0.3 µg m^{-2} s^{-1} (Figure 21b).

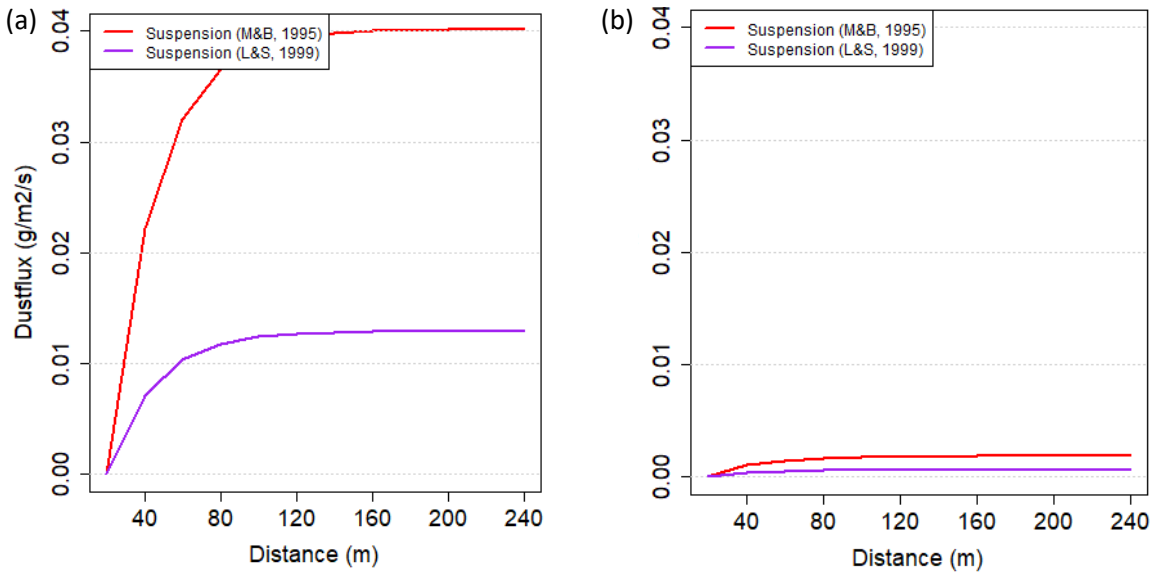

Figure 19. Dust flux for 2 dust schemes at the research site for a) bare conditions and b) water harvesting without grass conditions. Modelled for selected wind speed (14.89 m s^{-1} at 10m height) at 25-10-2018.

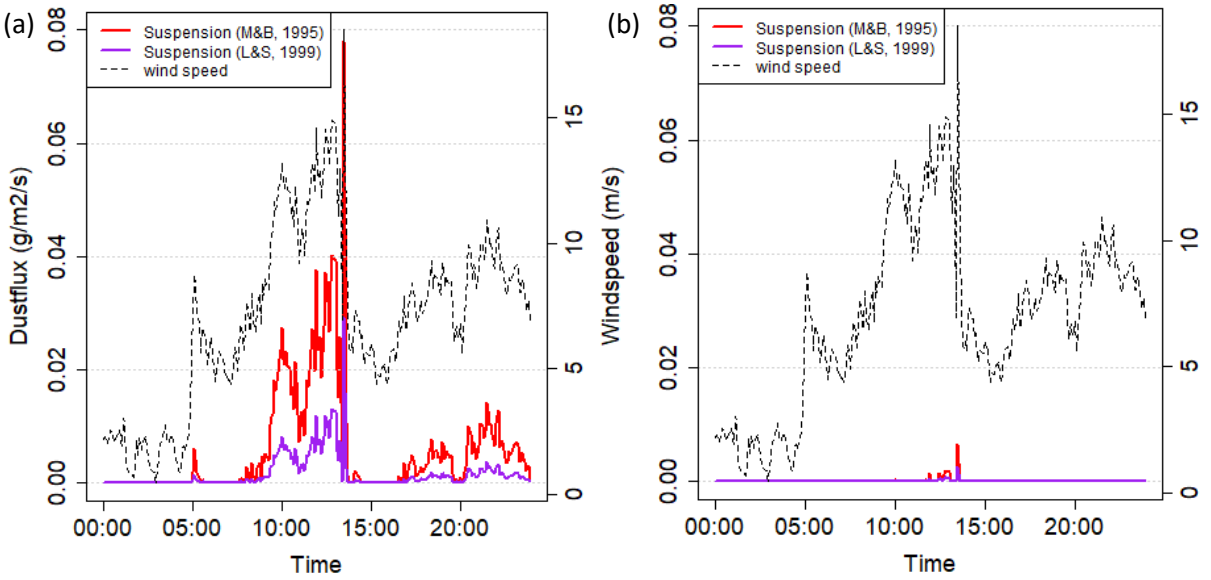

Figure 20. Dust flux for 2 dust schemes in last cell of the plot at the research site for a) bare conditions and b) water harvesting without grass conditions over 24 hours on 25-10-2018.

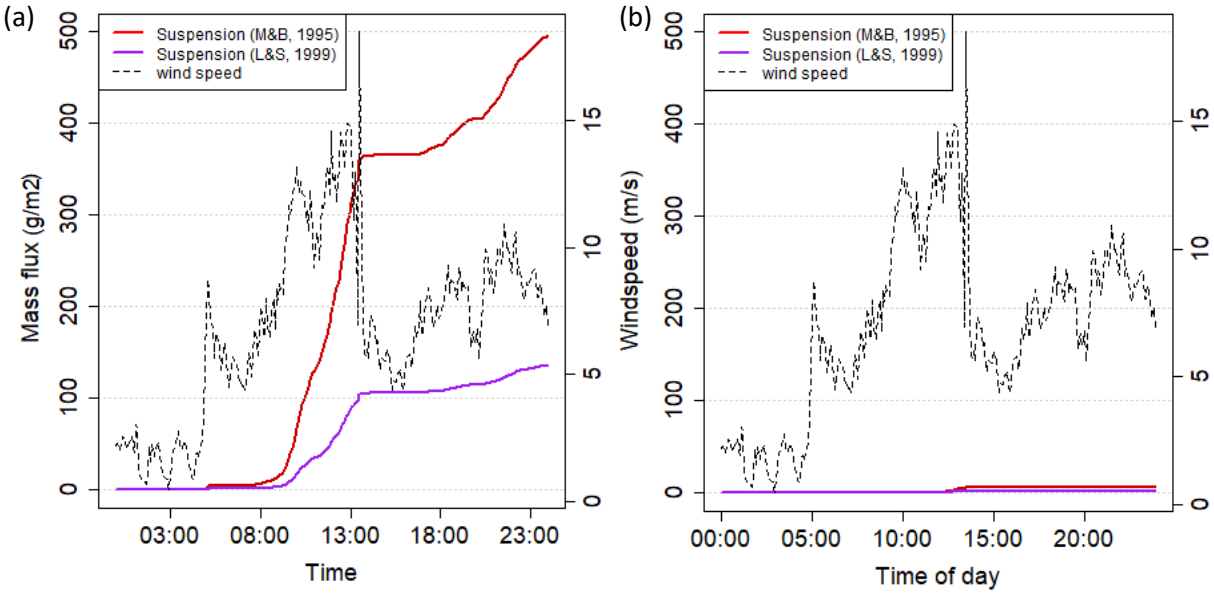

Figure 21. Cumulative suspension for 2 dust schemes in last cell of the plot at the research site for a) bare conditions and b) water harvesting without grass conditions over 24 hours on 25-10-2018.

4.4. RAMS-ICLAMS

4.4.1. Dust reduction

Large scale dust production simulations were done for 7 consecutive days to ensure appropriate initial and boundary conditions. The focus of the results here are for 25-10-2018 and 26-10-2018, and show the results of the inner domain. Figure 22 shows the modelled dust concentration near the surface on 25-10-2018 at 13:00h, for both the current conditions (a) and with water harvesting in suitable areas (b). The largest dust concentrations occur in the north (Syria), mid-west (Jordan-Saudi-Arabia border) and west (southern Israel), with the highest values ranging between 800 and 1000 µg m^{-3}. There is a clear difference between the current conditions and the WH conditions, with a reduction visible in the latter. From these figures, the strongest reductions are obtained in the Jordan

and southern Syria areas. Figure 23a confirms this by showing the absolute difference in dust concentration between the current conditions and the water harvesting scenario for a specified date and time. Red colours indicate reductions in the amount of dust, blue colours indicate an increase in the amount of dust. The largest absolute reductions are between 400 and 500 µg m^{-3}. Relative reductions (in percentage) for the same date and time are shown in Figure 23b. There is a large area of reduction visible in the east, but this is due to reductions of already low dust concentrations and is therefore less interesting. The Jordan-Syria area that shows large absolute reductions also shows large relative reductions (around 60-100%). Although these high percentages are for some parts also due to areas that had initially low dust concentrations, a large part of the area shows important decreases in places where dust concentration was high under current conditions, as seen in Figure 22. The areas with the largest reductions (both absolute and relative) correspond to the areas with the water harvesting structures (Figure 11), providing a good indication of the effect of these structures on dust production.

Considering the whole modelled area, the relative reduction ranges between 20 and 35%. Figure 24 shows the mean relative reduction over time for the whole area, which is determined as the relative difference between the sum of the total dust concentration in the current conditions and the water harvesting scenario in the whole area. These values are lower than the 60-100% reductions in the WH areas, as there are also large parts without these structures, or regions with little to no dust production in general. The graph shows that the reduction is the highest during the day and lower during night hours. This pattern was expected, as dust concentrations are generally lower during nighttime, when wind speeds are also lower (Figure 25). Water harvesting structures reduce the wind speed in general, but stronger during the day, as also shown in Figure 25.

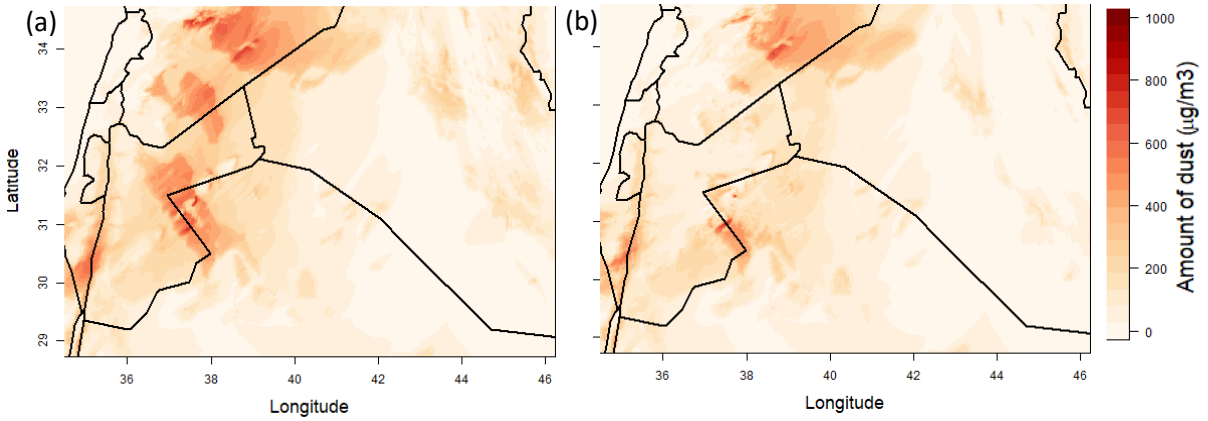

Figure 22. Modelled dust concentration near the surface on 25-10-2018, 13:00:00UTC for a) current conditions and b) water harvesting scenario. Animated version available in the Digital Appendix.

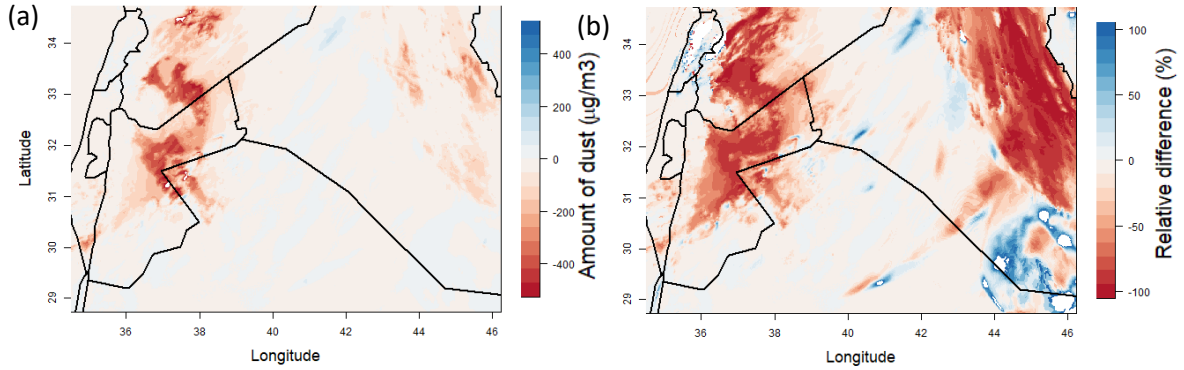

Figure 23. Differences in modelled dust concentration near the surface on 25-10-2018, 13:00:00UTC between current conditions and the water harvesting scenario: a) absolute dust concentration differences and b) relative dust concentration differences. Red colors indicate reduced values and blue colors indicate increased values. Animated version available in the Digital Appendix.

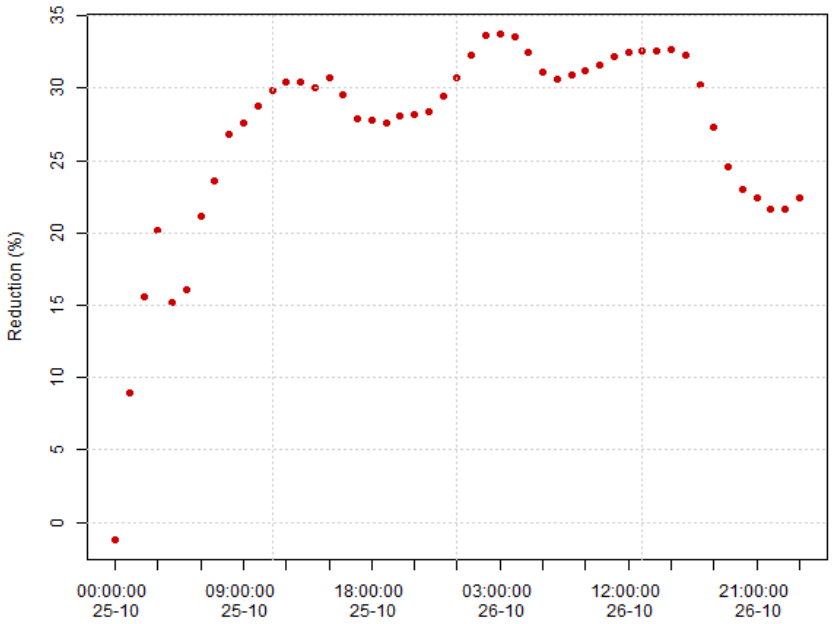

Figure 24. Mean relative reduction in dust concentration near the surface for the modelled region, from 25-10-2018 00:00:00 UTC to 27-10-2018 00:00:00 UTC.

4.4.2. Validation

The RAMS-ICLAMS simulation are based on weather data from ECMWF and model equations as described in section 3.1.2. To validate the resulting dust values and spatial pattern, a comparison was made with satellite imagery and PM_{10} measurements of the area.

MODIS imagery was used to compare the location of the modelled high dust concentration with actual visible dust storms. Because of high cloud cover on 25-10-2018, a satellite image of 26-10-2018

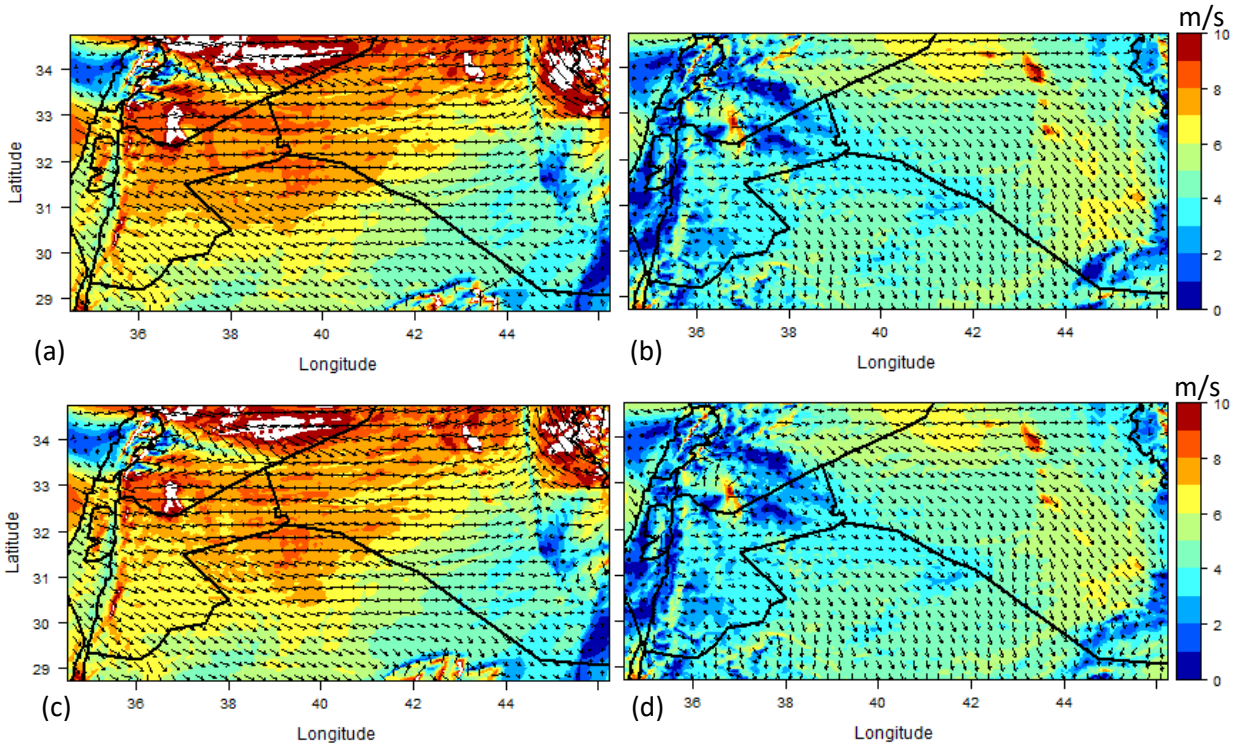

Figure 25. Modelled wind speed (m s^{-1}) and direction on 26-10-2018 for current conditions at a) 15:00:00 UTC and b) 23:00:00 UTC and water harvesting conditions for c) 15:00:00 UTC and d) 23:00:00 UTC. Animated version available in the Digital Appendix.

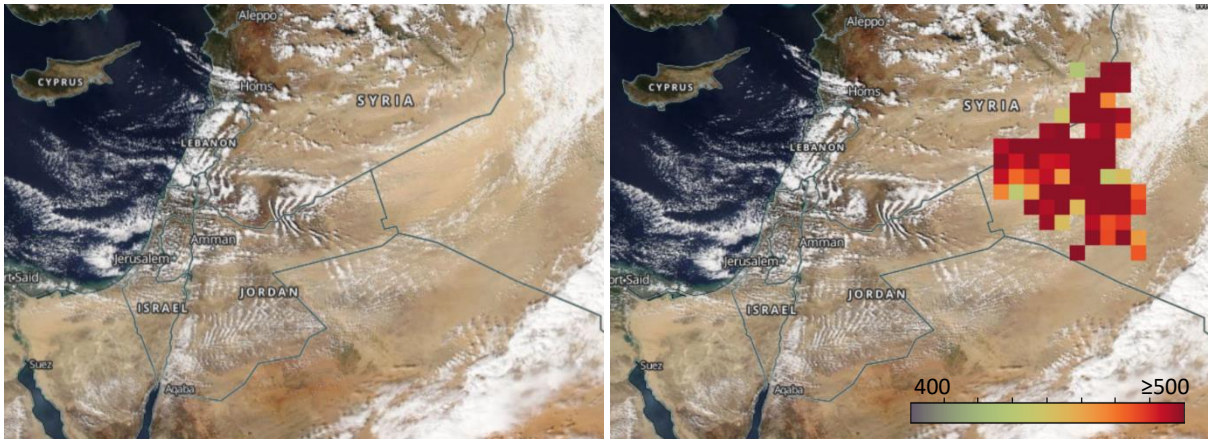

Figure 27. Dust storm over Iraq from Jordan direction on October 26, 2018, one day after model run date. Left: MODIS imagery with visible dust. Right: MODIS imagery with dust score based on radiances from infrared channels. Scores above 380 can indicate dust. (MODIS imagery retrieved from https://worldview.earthdata.nasa.gov/)

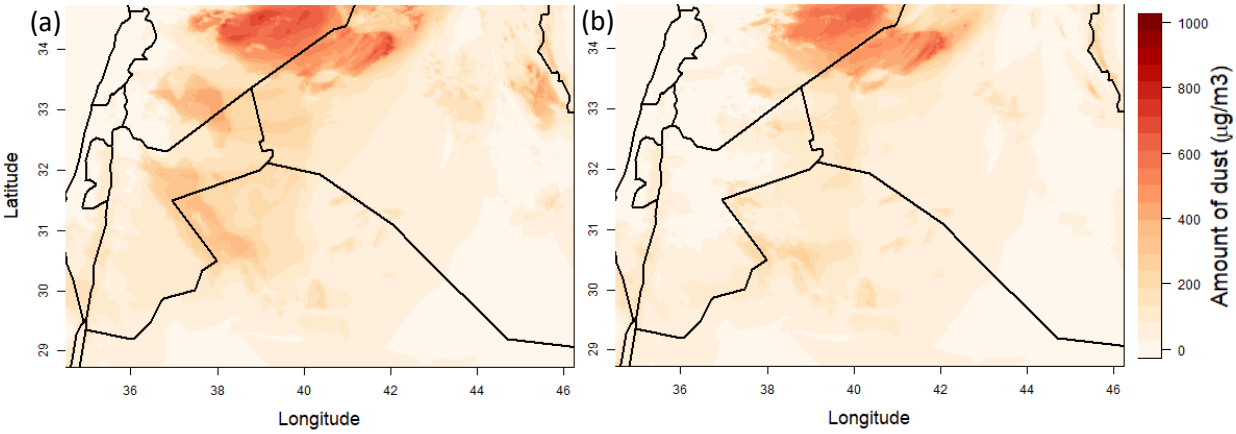

Figure 26. Modelled dust concentration near the surface on 26-10-2018, 13:00:00UTC for a) current conditions and b) water harvesting scenario.

was used instead. Figure 26 shows the surface reflectance (a) and the surface reflectance with a dust score (b). For reference, the maps of dust concentration near the surface of 26-10-2018 are given in Figure 27. It is clear that the location of the highest dust concentrations is modelled slightly higher to the northwest then the dust storm that occurred on that day. No dust score is given for areas in Jordan, but that is likely due to the cloud cover that is present, which inhibits a dust score assignment. Visually, some dust can be identified on the satellite image in the Jordan areas.

Data from Hussein et al. (2020) further confirms the presence of dust in the Amman area, as a dust episode was recorded between 23-10-2018 and 04-11-2018 with PM_{10} concentrations up to 190 µg m^{-3}. These values seem in a similar range as what is shown on the maps around Amman in both Figure 22 and Figure 27.

The aerodynamic roughness length that the model uses for the WH structures varies strongly from the roughness length used in the CASS model (Figure 28). RAMS-ICLAMS calculated the roughness length about 80 times higher: 0.395 m in the outscaled areas, as opposed to 0.005 m in CASS. This is mainly due to the 'Wooded grassland' land cover class, where the vegetation height and cover percentage are higher than what was modelled with CASS. These roughness values might be more accurate for fully developed and well-managed water harvesting structures, but the CASS model used values for relatively young structures, which were also the conditions in which the 2011 field measurements were performed (and therefore those correspond well).

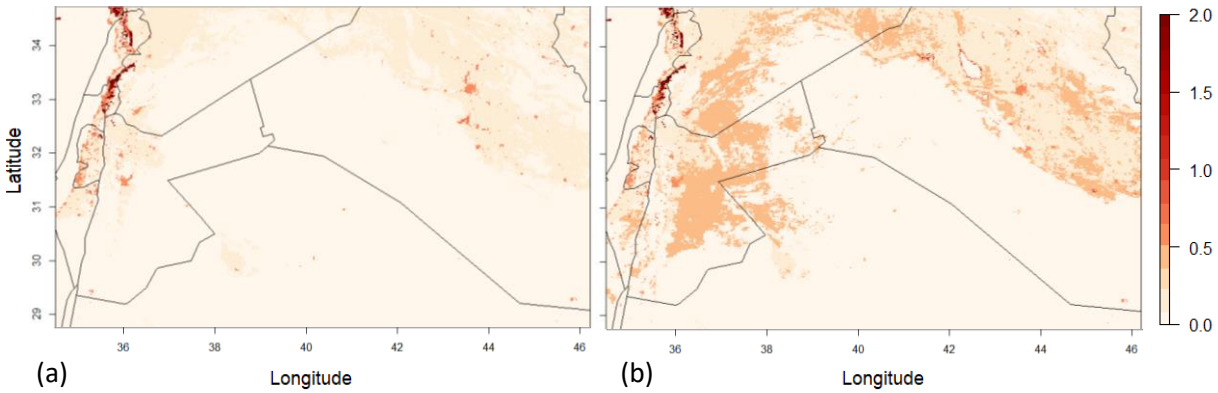

Figure 28. Modelled aerodynamic roughness length in the large scale study area for a) current conditions and b) water harvesting scenario.

5. Discussion

George Box famously stated: 'All models are wrong, but some are useful'. Models will never stop being limited, and especially in a complex scientific field such as the one of aeolian erosion, it will be long before all relevant processes are given a simplified representation in the form of physical equations. Currently more than eight of the most used wind erosion models vary in the most central approach and are all still unable to replicate field observations (Sherman, 2020). In this study, small scale and large scale wind erosion models were used to quantify erosion reduction by Vallerani water harvesting structures in the Jordanian Badia. Plot scale saltation and suspension reductions were investigated, as well as large scale dust production in the Badia environment and larger areas. The results show a strong effect when water harvesting conditions are implemented, with promising reductions in horizontal mass flux and dust production. However, the model limitations need to be considered when interpreting the results. Sherman (2020) outlined six of the strongest vexations about wind-blown sand in a thorough review paper, and all of them can be applied to this study. It doesn't mean it isn't useful, but limitations need to be considered when interpreting the results. Here, first the model findings will be compared to literature, then the model limitations are discussed and ideas for improvement and further research are suggested.

5.1. Transport reduction

The model runs performed in this study were simulations of wind speeds from October 25, 2018. This date was chosen because of a known dust storm that occurred this day, based on local media reports and visibility information from the wind data set. The wind speeds that day reached up to 18 m s^{-1}, specific results shown in this report are for a wind speed of ~15 m s^{-1}. The main findings are the reductions in transport for water harvesting conditions. Both the horizontal and vertical fluxes with WH conditions are reduced over 90%, with some transport equations even decreasing erosion by 99%. The simulations that were run for water harvesting with grass resulted in even stronger reductions than without grass (up to 100%, see Appendix A). The large scale RAMS-ICLAMS model reached reduction values of 30% for large areas and up to 100% in outscaled WH areas. Although there are still large dust areas visible, these are promising reduction values, that can significantly diminish environmental degradation and human health problems.

The erosion reductions obtained by CASS are high and partly due to the model set-up (section 5.2), but other studies have found values that near these extremes, albeit with varying conditions. Okin (2008) showed that the Raupach (1992) drag partitioning approach indeed has a strong reduction in horizontal flux with increasing λ, in a similar order of magnitude as values found here. They improved the model to incorporate the spatial distribution of the vegetation better, showing that an increase in λ does not lead to an as extreme reduction in horizontal flux. Dupont et al. (2014) compared the model by Okin (2008) with improvements in turbulent flow eddy modelling and their interactions with saltation processes, in the presence of various vegetation arrangements. They found that for increasing vegetation cover on loamy sands, the approach of Okin (2008) resulted in horizontal flux reductions from 37% up to 91%. With their improved model, Dupont et al. (2014) found for the same vegetation arrangements flux reductions of 51% to 89%. It should be noted that the highest reduction values found were for significantly larger vegetation cover and roughness density than were used in this paper's model. The lower end of the found values are therefore most representative to compare with the CASS model findings, as they were done for vegetation cover of 10% and λ of 0.044. The results do correspond more with the reductions found by RAMS, which also had a higher vegetation cover. However, the Dupont et al. (2014) model also included so-called 'streets': stretched patches of bare soil were wind has free play. With WH structures, these streets only exist when the wind direction becomes nearly perpendicular to the vegetation rows. This does happen in the contour line-following distribution of the Vallerani structures in the field, but is not modelled as such in this study, therefore also explaining the much higher reduction values found here. When it comes to

interpretation of these high values, the results of the above-mentioned studies are important to consider. As the approach of this model is similar to the original Raupach (1992) approach, which, with the Okin (2008) and Dupont et al. (2014) improvements, still led to reductions in horizontal flux of at least 37-51%, the high values obtained here may be overestimations, but still indicate that important reductions in horizontal and subsequently also vertical fluxes can be expected when water harvesting structures are implemented.

The absolute erosion values and reduction thereof are difficult to interpret as such, due to factors described in the next section. This makes it hard to quantify possible soil loss, but simple comparisons with field research can be made. For example, Klose et al. (2019) studied dust emissions from crusted surfaces by comparing field measurements with modelled values. They used the same dust emission scheme by Lu & Shao (1999) and saltation scheme by Kawamura (1964) for 5 (almost) bare soils ranging from sand to silty clay loam. Their results show a similar order of magnitude for both horizontal sediment flux (ranging between 0 and 8 g m^{-1} s^{-1} for an 8-hour period), and vertical dust flux (ranging between 0 and 100 µg m^{-2} s^{-1} over an 8-hour period). These main results were however for a site with sandy soils, indicating a small silt and clay fraction and thus relatively less material available for erosion (especially with crusting). The fact that their results are still similar to the CASS model results might be due to the relatively large grain diameter that was used in CASS: no intrinsic distinction was made between saltating and suspended particles. When the smaller particle size of clay particles (and the high clay fraction in the area) was taken into account, the dust flux from the CASS model may have been higher. The Klose et al. (2019) fluxes are also relatively high compared to the CASS model because they used a c_0 value of 7.6 for the Kawamura (1964) equation, based on a study by Shao et al. (2011), who set this value to match modelled sediment fluxes with observed sediment fluxes. This automatically leads to larger fluxes, as explained in section 5.2.

Sterk et al. (1999) compared two different tillage treatments on a silt loam soil in Spain (with similar soil characteristics as the Al Majidiyya site). They compared the effects of conventional deep ploughing with reduced shallow ploughing during 4 wind erosion events of several hours. They didn't find significant soil loss for the reduced tillage and calculated a sediment loss of 0.5 ton ha^{-1} for the conventional tillage; amounts that don't indicate severe soil loss. The found values of 1.97 ton ha^{-1} for the erosion event on bare soil modelled in this study are slightly higher, but still comparable. Furthermore, Sterk et al. (1999) also found that severe crusting occurred in their north-eastern Spain research area due to strong intense rainfall events during the field study. Rainfall in that study area was generally higher than in the Jordanian Badia (365 mm vs. ±150 mm), making erosion under similar circumstances in the Badia likely higher. According to Morgan (2009) soil erosion is moderate between 5-10 ton ha^{-1} y^{-1} and becomes severe over 50 ton ha^{-1} y^{-1}. The severity of the soil loss problem is thus dependent on the number of dust events that occur, but also on average wind speeds, as erosion can occur even under low(er) wind speeds. However, even if the local soil loss might not be a large issue, the effects of dust on the climate and human health can nevertheless be significant and reductions of erosion are still needed. The reduction under water harvesting conditions of over 88% are therefore still important to emphasize the WH ecosystem service and justify the implementations of these structures. Gomes et al. (2003) expanded the research of Sterk et al. (1999) to include the vertical dust flux and found values between 0.4-70 µg m^{-2} s^{-1} for the conventional tillage: in the same range as the values obtained with CASS. Although these studies looked at tillage treatments and not vegetation, the correspondence of the bare soil fluxes do confirm the fluxes calculated by CASS, as the soil characteristics are comparable. The effect of water harvesting structures therefore also seem more trustworthy, and an adequate measure to reduce the both the horizontal and vertical mass fluxes.

Similar reductions through vegetation were obtained by Sterk et al. (2012) during a study on a sandy soil in Central Patagonia, where they investigated sediment fluxes on plots with or without windbreaks and/or cherry trees. Here, soil loss ranged from 1.6-148.7 ton ha^{-1} for storms ranging from 4 to 20 hours on a bare sandy soil, and were reduced by 51% for windbreak plots and practically 100% for cherry tree plots. As the cherry trees were placed in a similar spatial pattern as Vallerani WH

structures, these reductions seem to correspond with findings of this study. However, as the trees are larger and soil characteristics are very different, a true comparison remains difficult.

Where the study by Klose et al. (2019) used a much larger c_0 value for calculations then used in CASS, the study by Sterk et al. (2012) obtained c_0 values from field measurements that were again much smaller. Although none of the values used are necessarily inaccurate, these fundamental differences complicate direct flux comparison. The 'baseline' bare soil scenario in both the Klose et al. (2019) and Sterk et al. (2012) study differ too much from the current study to say something about the absolute horizontal and vertical sediment fluxes. It does however underline the large reducing effect vegetation (and in this case water harvesting structures) can have on mass flux values. It does also highlight the need for validation with field measurements for each individual modelling study, as no wind erosion scenario is the same.

5.2. Model limitations

When interpreting the results, the modelled conditions need to be kept in mind. The CASS model results show strong reductions in both horizontal and vertical fluxes, but as the model is run under ideal circumstances where the wind is blowing over horizontal surfaces and exactly perpendicular to the water harvesting rows, the extent of the reductions might be an overestimation. In reality, when the wind is blowing from various angles and over sloping terrain, the roughness that the wind experiences will vary, and with that also the transport fluxes (as shown in Figure 18b).

The c_0 coefficients in the transport equations are a large source of uncertainty. Values given for the original equations are of the order 10^0, but Sterk et al. (2012) obtained values in the order of 10^{-2}-10^{-1}. As this value is an indicator of the erodibility of the soil, it needs to be calibrated with field measurements to get an accurate expression for this empirical constant, especially when soil moisture variation or crusting play a role. The values chosen for c_0 strongly influence the size of the flux, as it is directly multiplied by the rest of the equation. For example, if the recommended value of the coefficient in the original Kawamura equation is used (which was 4.2), the resulting flux would be 40 times larger than what was found with the value used in this study. Clearly, this indicates that the quantity of all fluxes found in this paper are not to be taken as true values. The focus should rather lie on the relation between the fluxes under bare conditions and under water harvesting conditions, as these remain consistent no matter what coefficient value is used. As described in section 5.1, these can lead to strong reductions in horizontal transport and dust production.

Next, deposition is not modelled explicitly. For creep and saltation, deposition is strongly influenced by vegetation, and therefore spatially dependent. For short and long term suspension, deposition occurs through both dry and wet deposition and is slightly less influenced by vegetation as it can be transported at larger heights (Okin et al., 2006; Shao, 2008). It is also more dependent on particle diameter, settling velocities and turbulence, which are not explicitly considered in this study (Raupach & Lu, 2004). Although a net erosion plot is given (Figure 18a) this is merely a derivative of the calculated fluxes between cells, not a physically derived calculation. Including deposition could therefore alter the obtained fluxes. However, the RAMS model does include various depositional mechanisms, and still obtains high flux reductions. This confirms the reduction values calculated by the CASS model.

One of the driving factors in all transport equations and subsequently the results is the vegetation frontal density (λ) (*3.3*), first introduced by Marshall (1971) and further worked out by Raupach (1992). In the CASS model, the required vegetation values are calculated per cell, giving average values over 20 m, which are used in further calculations (as represented in Figure 9). With this approach, the spatial distribution of vegetation is not taken into account, and vegetation settings with large height but low ground cover will results in similar horizontal transport fluxes as vegetations settings with smaller height and larger ground cover. However, the different spatial distributions of the vegetation have been shown to have different fluxes in reality (Dupont et al., 2014; Okin & Gillette, 2001; Webb et al., 2014), with lower fluxes for denser, shorter objects. This issue is also referred to as the

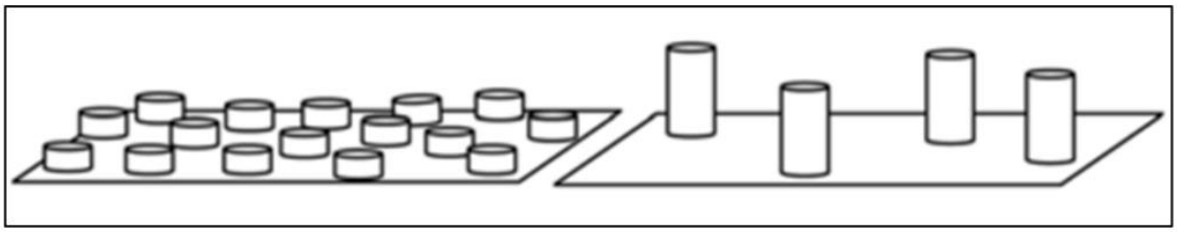

Figure 29. Problem of frontal area index λ: both situations have the same λ and therefore the same horizontal flux, but intuitively this is not accurate. From: Okin (2008).

'Telephone Pole Problem' (Figure 29) (Mayaud & Webb, 2017; Okin, 2008). This is especially relevant in case of low vegetation cover, as more bare soil is available for erosion. Because of the low vegetation density and the even spacing between water harvesting rows, wind speeds can develop over the interrow space and initiate transport. However, because the values for λ are large, total drag is disproportionally partitioned onto the vegetation, leaving little friction velocity to erode the surface. This effect is amplified when including grass in the simulations, as the many blades of grass are mathematically distributed throughout the area, instead of located at concentrated zones. Although grass has in multiple studies been shown to have a strong reducing factor (Li et al., 2007; Mayaud et al., 2016) and has in previous research with the CASS model been shown to be the most effective in reducing wind erosion (Smeets, 2020), the spatial distribution of the grass in the model would in the field not lead to such strong reductions. It is therefore likely that the effect of the sparse vegetation (for shrubs and/or grasses) on the total transport in the model is overestimated, and the reduction of the flux therefore as well (Figure 15). This issue was not as clear in RAMS, as in a grid size of 100x100 m values are automatically averaged. This was also initially the reason to integrate these two models, to get the small scale representation in a large scale model. Because the coupling of the two models was not as thorough as planned in advance, due to time limitations, the adjustments were mainly made through the use of the 'Wooded grassland' land cover class. This did however also lead to high roughness length values and therefore also high reduction values. These values provide a good insight into mass fluxes in fully developed water harvesting areas, and indicate strong decreases in dust productions, but they are more difficult to compare with the CASS results for this reason. The spatial variation of net erosion (as seen in Figure 18a) is also likely to vary more on the plot scale, with repeating zones of erosion and deposition, depending on the location relative to the vegetation. However, the overall erosion reduction values obtained are still valid for the macro scale and remains promising in lowering the negative effects of soil loss and dust production.

5.3. Further research

Although bare soil and water harvesting simulations provide valuable insights into current and possible future scenarios, barley conditions have not been modelled. Exploring this would be valuable, as many natural plots have been converted for barley harvesting, which may be more degrading to the environment due to inappropriate cultivation. With seasonal ploughing and crust breaking, creation of ridges and the barley vegetation cycle, these conditions have a whole different influence on wind erosion, both enhancing and reducing it depending on the season. In this case, replacing it by water harvesting might also be promising, although there is likely a delicate balance between food production for human consumption and growing for livestock fodder. Furthermore, if barley is replaced by water harvesting, overgrazing becomes a larger problem, as there is less food available for animals. Close management of WH areas is therefore required.

This small-scale, but basic, model can be improved in several ways. The cell size was chosen based on the governing equations: the scale of the experimental wind-tunnel set-ups that were the base for the derivations of the formulas were in the order of 10-100 m (Dong et al., 2003; White, 1979; Zingg, 1953). Going to a smaller grid size would be preferable, as it would allow for better incorporation of the vegetation spatial distribution, but it raises the question of the applicability of the formulas. If field

measurements can be performed, the model set-up could be validated on an even smaller scale and thus represent the Vallerani water harvesting structures better. If this is done, important processes can also be included, such as the downwind wake of the vegetation. As roughness elements absorb momentum from the wind, the wind speeds are reduced in the wake zone behind the element (Hong et al., 2020), which in turn can lead to a decrease of the sediment fluxes. At the same time, the turbulence is altered, possibly leading to an increase of sediment fluxes under certain vegetation covers (Dupont et al., 2013; Mayaud & Webb, 2017). In Appendix B an altered version of the CASS model can be found, using a cell size of 1 m and including more accurate spatial vegetation distribution. The results from the altered model seem more in line with intuitively correct flux patterns, as can be expected with a smaller spatial scale. As noted before, validation with field measurements is necessary to verify the used equations and found values, but this improved model is a good starting point for further research.

The integration with the large scale RAMS-ICLAMS model can be deepened by creating a new land cover class with exactly the parameters that are obtained from the small scale model. For example, roughness length can be forced with the small scale model values, instead of calculated, as calculations on the RAMS-ICLAMS cell size of 100 m encounter the same issues as with the CASS cell size of 20 m: the hetereogeneity of the surface is lost. The forcing of these parameters enables an even better estimation of dust reductions on a regional scale.

6. Conclusion

The aim of this study was to assess the effect of Vallerani water harvesting structures on aeolian erosion and dust production in the Jordanian Badia. It addressed both the plot scale and regional scale effects, by modelling horizontal and vertical sediment fluxes and reductions thereof under water harvesting conditions. The field scale model was coupled with a large scale dust production model to simulate creep, saltation and suspension fluxes in the Badia environment, in order to quantify reductions in wind erosion and dust production. From the main aim and the related research questions some conclusions can be made.

On the plot scale, there are many different approaches to take when it comes to model set-up. The five transport equations used in the CASS model result in similar patterns, but the magnitudes of the fluxes are heavily relying on empirical coefficients that need field validation. Although this complicates interpretation of absolute values, the relative effect of implementing water harvesting techniques is still valid.

Based on plot scale modelling as done in this study, water harvesting is a promising technique for wind erosion reduction. For erosion events in the Jordanian Badia it showed reductions in both horizontal and vertical sediment fluxes of over 90% under ideal conditions, thereby strongly lessening the negative effects on the environment and human health. When wind direction angles are taken into consideration with water harvesting structures, it is shown that small angles do not influence the erosion strongly, whereas with larger angles erosion increases towards bare soil flux values.

On a large scale, outscaling water harvesting techniques can also lead to reductions in dust productions up to 100% locally. On average for the modelled region it resulted in a reduction of 30%, which is significant when considering that large areas where little to no dust is produced are also included in this number.

An important limitation of the CASS model is the use of the vegetation frontal density, creating a Telephone Pole Problem where different vegetation settings can lead to equal horizontal fluxes. This can be improved by decreasing the cell size, but field validation of modelled fluxes is then necessary to confirm the applicability of the used transport equations. Further research should focus on expanding the model with better implementation of this vegetation spatial distribution. It should also look at different conditions that are found in the Badia, such as barley harvesting that occurs on a large scale. Improved implementation of the obtained parameters in the RAMS-ICLAMS model can be done by developing a specific water harvesting land use class. Proposed upgrades can give even more precise insight into aeolian erosion reductions through Vallerani water harvesting structures and the positive effects this will have on the environment and human health.

References

Abu Sada, A., Abu-Allaban, M., & Al-Malabeh, A. (2015). Temporal and Spatial Analysis of Climate Change at Northern Jordanian Badia. *Jordan Journal of Earth and Environmental Sciences*, *7*(2), 87–93.

Akimoto, K. (2021). *Relationships between soil properties, soil moisture and vegetation recovery status at a micro catchment water harvesting adopted site in Jordan's Badia*. MSc Thesis. Tottori University.

Al-Homoud, A. S., Allison, R. J., Sunna, B. F., & White, K. (1995). Geology, Geomorphology, Hydrology, Groundwater and Physical Resources of the Desertified Badia Environment in Jordan. *GeoJournal*, *37*(1), 51–67.

Ali, A, & Yazar, A. (2007). Effect of Micro-catchment water harvesting on soil-water storage and shrub establishment in the arid environment. *International Journal of Agriculture & Biology*, *9*(2), 302–306. Retrieved from http://www.fspublishers.org/published_papers/4992_..pdf

Ali, Akhtar, Oweis, T., Aal, A. A., Mudabbar, M., Zubaidi, K., & Bruggeman, A. (2006). The Vallerani Water Harvesting System, (23), 13–15.

Ali, Akhtar, Yazar, A., Abdul Aal, A., Oweis, T., & Hayek, P. (2010). Micro-catchment water harvesting potential of an arid environment. *Agricultural Water Management*, *98*(1), 96–104. https://doi.org/10.1016/j.agwat.2010.08.002

Bagnold, R. A. (1941). *The Physics of Blown Sand and Desert Dunes*. Methuen, New York.

Chen, P. S., Tsai, F. T., Lin, C. K., Yang, C. Y., Chan, C. C., Young, C. Y., & Lee, C. H. (2010). Ambient influenza and avian influenza virus during dust storm days and background days. *Environmental Health Perspectives*, *118*(9), 1211–1216. https://doi.org/10.1289/ehp.0901782

Cooke, R. U., & Warren, A. (1973). *Geomorphology in deserts*. University of California Press.

Dong, Z., Liu, X., Wang, H., & Wang, X. (2003). Aeolian sand transport: A wind tunnel model. *Sedimentary Geology*, *161*(1–2), 71–83. https://doi.org/10.1016/S0037-0738(02)00396-2

Duijts, C. (2012). *Modelling aeolian sediment transport in the Badia of Jordan*. MSc Thesis. Utrecht University.

Dupont, S., Bergametti, G., Marticorena, B., & Simoëns, S. (2013). Modeling saltation intermittency. *Journal of Geophysical Research Atmospheres*, *118*(13), 7109–7128. https://doi.org/10.1002/jgrd.50528

Dupont, S., Bergametti, G., & Simoëns, S. (2014). Modeling aeolian erosion in presence of vegetation. *Journal of Geophysical Research : Earth Surface*, *119*, 168–187. https://doi.org/10.1002/2013JF002875.Received

ESA. (2017). *Land Cover CCI Product User Guide Version 2*. Technical Report. Retrieved from maps.elie.ucl.ac.be/CCI/viewer/download/ESACCI-LC-Ph2-PUGv2_2.0.pdf

Favis-Mortlock, D. (2004). Self-Organization and Cellular Automata Models. In J. Wainwright & M. Mulligan (Eds.), *Environmental Modelling: Finding Simplicity in Complexity* (pp. 45–68). John Wiley & Sons, Ltd.

Fécan, F., Marticorena, B., & Bergametti, G. (1998). Parametrization of the increase of the aeolian erosion threshold wind friction velocity due to soil moisture for arid and semi-arid areas. *Annales Geophysicae*, *17*(1), 149–157. https://doi.org/10.1007/s00585-999-0149-7

Field, J. P., Belnap, J., Breshears, D. D., Neff, J. C., Okin, G. S., Whicker, J. J., … Reynolds, R. L. (2010). The ecology of dust. *Frontiers in Ecology and the Environment*, *8*(8), 423–430. https://doi.org/10.1890/090050

Fryrear, D. W., & Skidmore, E. L. (1985). Methods for Controlling Wind Erosion. *Soil Erosion and Crop Productivity*, 443–457. https://doi.org/10.2134/1985.soilerosionandcrop.c24

Gammoh, I. A., & Oweis, T. Y. (2011). Performance and Adaptation of the Vallerani Mechanized Water Harvesting System in Degraded Badia Rangelands. *Journal of Environmental Science and Engineering*, *5*(October), 1370–1380. Retrieved from http://www.davidpublisher.org/Public/uploads/Contribute/55278f4be0cae.pdf

Gillette, D. A. (1977). Fine particulate emissions due to wind erosion. *Trans. Am. Soc. Agric. Eng.*, *20*, 890–987.

Gomes, L., Arrúe, J. L., López, M. V., Sterk, G., Richard, D., Gracia, R., … Frangi, J. P. (2003). Wind erosion in a semiarid agricultural area of Spain: The WELSONS project. *Catena*, *52*(3–4), 235–256. https://doi.org/10.1016/S0341-8162(03)00016-X

Goudie, A. S. (2014). Desert dust and human health disorders. *Environment International*, *63*, 101–113. https://doi.org/10.1016/j.envint.2013.10.011

Grant, P. F., & Nickling, W. G. (1998). Direct field measurement of wind drag on vegetation for application to windbreak design and modelling. *Land Degradation and Development*, *9*(1), 57–66. https://doi.org/10.1002/(SICI)1099-145X(199801/02)9:1<57::AID-LDR288>3.0.CO;2-7

Hong, C., Chenchen, L., Xueyong, Z., Huiru, L., Liqiang, K., Bo, L., & Jifeng, L. (2020). Wind erosion rate for vegetated soil cover: A prediction model based on surface shear strength. *Catena*, *187*(19), 104398. https://doi.org/10.1016/j.catena.2019.104398

Hussein, T., Li, X., Al-Dulaimi, Q., Daour, S., Atashi, N., Viana, M., … Petäjä, T. (2020). Particulate Matter Concentrations in a Middle Eastern City – an insight to Sand and Dust Storm Episodes. *Aerosol Air Quality Research*. https://doi.org/https://doi.org/10.4209/aaqr.2020.05.0195

IPCC. (2019). *Climate Change and Land Ice; IPCC Special Report on climate change, desertification, land degradation, sustainable land management, food security, and greenhouse gas fluxes in terrestrial ecosystems*. (P. R. Shukla, J. Skea, E. Calvo Buendia, C. Masson-Delmotte, H.-O. Pörtner, D. C. Roberts, … J. Malley, Eds.). https://doi.org/10.1002/9781118786352.wbieg0538

Janjic, Z. I. (1984). Nonlinear Advection Schemes and Energy Cascade on Semi-Staggered Grids. *Monthly Weather Review*, *112*(6), 1234–1245.

Karrou, M., Oweis, T., Ziadat, F., & Awawdeh, F. (Eds.). (2011). *Rehabilitation and integrated management of dry rangelands environments with water harvesting*. *Community-based optimization of the management of scarce water resources in agriculture in Central and West Asia and North Africa Report no. 9.* ICARDA, Alepo, Syria.

Kawamura, R. (1964). *Study on Sand Movement by Wind*. *Hydraulic Engineering Laboratory Tech. Rep.* Berkely, CA.

Kind, R. J. (1976). A critical examination of the requirements for model simulation of wind-induced erosion/deposition phenomena such as snow drifting. *Atmospheric Environment*, *10*(3), 219–227. https://doi.org/10.1016/0004-6981(76)90094-9

Klose, M., Gill, T. E., Etyemezian, V., Nikolich, G., Ghodsi, Z., Webb, N. P., & Pelt, R. S. Van. (2019). Dust emission from crusted surfaces: Insights from field measurements and modelling. *Aeolian Research*, *40*, 1–14. https://doi.org/10.1016/j.aeolia.2019.05.001

Kok, J. F., Parteli, E. J. R., Michaels, T. I., & Karam, D. B. (2012). The physics of wind-blown sand and dust. *Reports on Progress in Physics*, *75*(10). https://doi.org/10.1088/0034-4885/75/10/106901

Kottek, M., Grieser, J., Beck, C., Rudolf, B., & Rubel, F. (2006). World map of the Köppen-Geiger climate classification updated. *Meteorologische Zeitschrift*, *15*(3), 259–263. https://doi.org/10.1127/0941-2948/2006/0130

Lettau, K., & Lettau, H. H. (1978). Experimental and micrometeorological field studies of dune migration. *Exploring in the World's Driest Climate*, 110–147.

Li, J., Okin, G. S., Alvarez, L., & Epstein, H. (2007). Quantitative effects of vegetation cover on wind erosion and soil nutrient loss in a desert grassland of southern New Mexico, USA. *Biogeochemistry*, *85*(3), 317–332. https://doi.org/10.1007/s10533-007-9142-y

Lu, H., & Shao, Y. (1999). A new model for dust emission by saltation bombardment. *Journal of Geophysical Research Atmospheres*, *104*(D14), 16827–16842. https://doi.org/10.1029/1999JD900169

Maegley, W. J. (1976). Saltation and Martian Sandstorms. *Review of Geophysics and Space Physics*, *14*(I), 135–142.

Mahowald, N. M., Engelstaedter, S., Luo, C., Sealy, A., Artaxo, P., Benitez-Nelson, C., … Siefert, R. L. (2009). Atmospheric iron deposition: Global distribution, variability, and human perturbations. *Annual Review of Marine Science*, *1*, 245–278. https://doi.org/10.1146/annurev.marine.010908.163727

Marshall, J. K. (1971). Drag measurements in roughness arrays of varying density and distribution. *Agricultural Meteorology*, *8*, 269–292.

Marticorena, B., & Bergametti, G. (1995). Modeling the atmospheric dust cycle: 1. Design of a soil-derived dust emission scheme. *Journal of Geophysical Research*, *100*(D8). https://doi.org/10.1029/95jd00690

Mayaud, J. R., & Webb, N. P. (2017). Vegetation in drylands: Effects on wind flow and aeolian sediment transport. *Land*, *6*(3), 31–33. https://doi.org/10.3390/land6030064

Mayaud, J. R., Wiggs, G. F. S., & Bailey, R. M. (2016). Characterizing turbulent wind flow around dryland vegetation. *Earth Surface Processes and Landforms*, *41*(10), 1421–1436. https://doi.org/10.1002/esp.3934

Mesinger, F., Janjic, Z. I., Nickovic, S., Gavrilov, D., & Deaven, D. G. (1988). The step-mountain coordinate: Model description and performance for cases of Alpine lee cyclogenesis and for a case of an Appalachian redevelopment. *Monthly Weather Review*, *116*(7), 1493–1518.

Morgan, R. P. C. (2009). *Soil Erosion and Conservation*. Blackwell Publishing Ltd.

NASA/METI/AIST/Japan Spacesystems, & U.S./Japan ASTER Science Team. (2018). ASTER Global Digital Elevation Model V003 [Data Set]. *NASA EOSDIS Land Processes DAAC*.

Nickovic, S., Kallos, G., Papadopoulos, A., & Kakaliagou, O. (2001). A model for prediction of desert dust cycle in the atmosphere. *Journal of Geophysical Research: Atmospheres*, *106*(D16), 18113–18129. https://doi.org/10.1029/2000JD900794

Okin, G. S., Gillette, D. A., & Herrick, J. E. (2006). Multi-scale controls on and consequences of aeolian processes in landscape change in arid and semi-arid environments. *Journal of Arid Environments*, *65*(2), 253–275. https://doi.org/10.1016/j.jaridenv.2005.06.029

Okin, G S, & Gillette, D. A. (2001). Distribution of vegetation in wind-dominated landscapes: Implications for wind erosion modeling and landscape processes. *Journal of Geophysical Research Atmospheres*, *106*(D9), 9673–9683. https://doi.org/10.1029/2001JD900052

Okin, Gregory S. (2008). A new model of wind erosion in the presence of vegetation. *Journal of Geophysical Research: Earth Surface*, *113*(2), 1–11. https://doi.org/10.1029/2007JF000758

Oweis, T., Prinz, D., & Hachum, A. (2001). *Water Harvesting: Indigenous Knowledge for the Future of the Drier Environments*. ICARDA, Aleppo, Syria.

Oweis, T. Y. (2017). Rainwater harvesting for restoring degraded dry agro-pastoral ecosystems: A conceptual review of opportunities and constraints in a changing climate. *Environmental Reviews*, *25*(2), 135–149. https://doi.org/10.1139/er-2016-0069

Presley, D., & Tatarko, J. (2009). Principles of Wind Erosion and its Control. *Kansas State University Research and Extension*, (MF-2860). Retrieved from http://scholar.google.com/scholar?hl=en&btnG=Search&q=intitle:Principles+of+Wind+Erosion+and+its+Control#0

Raupach, M. R. (1992). Drag and drag partition on rough surfaces. *Boundary-Layer Meteorology*, *60*(4), 375–395. https://doi.org/10.1007/BF00155203

Raupach, Michael R., & Lu, H. (2004). Representation of land-surface processes in aeolian transport models. *Environmental Modelling and Software*, *19*(2), 93–112. https://doi.org/10.1016/S1364-8152(03)00113-0

Sarcinella, M. (2020). *Arid land rehabilitation technology in the Jordan Badia: potential for out-scaling rainwater harvesting*

practices. MSc Guided Research. Utrecht University.
Sarre, R. D. (1987). Aeolian sand transport. *Progress in Physical Geography*, *11*(2), 157–182.
Shao, Y., Raupach, M. R., & Findlater, P. A. (1993). Effect of Saltation Bombardment on the Entrainment of Dust by Wind. *Journal of Geophysical Research*, *98*(D7). https://doi.org/10.1029/93jd00396
Shao, Y, Ishizuka, M., Mikami, M., & Leys, J. F. (2011). Parameterization of size - resolved dust emission and validation with measurements, *116*(May 2010), 1–19. https://doi.org/10.1029/2010JD014527
Shao, Yaping. (2004). Simplification of a dust emission scheme and comparison with data. *Journal of Geophysical Research D: Atmospheres*, *109*(10), 1–6. https://doi.org/10.1029/2003JD004372
Shao, Yaping. (2008). *Physics and Modelling of Wind Erosion*. *Atmospheric and Oceanographic Sciences Library*. https://doi.org/10.1007/978-1-4020-8895-7_4
Shao, Yaping, & Lu, H. (2000). A simple expression for wind erosion threshold friction velocity. *Journal of Geophysical Research*, *105*, 22437–22443.
Sherman, D. J. (2020). Understanding wind-blown sand: Six vexations. *Geomorphology*, *366*, 107193. https://doi.org/10.1016/j.geomorph.2020.107193
Sherman, D. J., Jackson, D. W. T., Namikas, S. L., & Wang, J. (1998). Wind-blown sand on beaches: An evaluation of models. *Geomorphology*, *22*(2), 113–133. https://doi.org/10.1016/S0169-555X(97)00062-7
Smeets, T. (2020). *Drought and effect of vegetation on aeolian transport in the Aralkum*. MSc Thesis. Utrecht University.
Soleimani, Z., Teymouri, P., Darvishi Boloorani, A., Mesdaghinia, A., Middleton, N., & Griffin, D. W. (2020). An overview of bioaerosol load and health impacts associated with dust storms: A focus on the Middle East. *Atmospheric Environment*, *223*(July 2019), 117187. https://doi.org/10.1016/j.atmosenv.2019.117187
Spyrou, C., Kallos, G., Mitsakou, C., Athanasiadis, P., Kalogeri, C., & Iacono, M. J. (2013). Modeling the radiative effects of desert dust on weather and regional climate. *Atmos. Chem. Phys*, *13*, 5489–5504. https://doi.org/10.5194/acp-13-5489-2013
Spyrou, C., Mitsakou, C., Kallos, G., Louka, P., & Vlastou, G. (2010). An improved limited area model for describing the dust cycle in the atmosphere. *Journal of Geophysical Research Atmospheres*, *115*(17), 1–19. https://doi.org/10.1029/2009JD013682
Sterk, G. (2003). Causes, consequences and control of wind erosion in Sahelian Africa: A review. *Land Degradation and Development*, *14*(1), 95–108. https://doi.org/10.1002/ldr.526
Sterk, G, López, M. V, & Arrúe, J. L. (1999). Saltation Transport On A Silt Loam Soil in Northeast Spain. *Land Degradation & Development*, *10*, 545–554.
Sterk, Geert, Parigiani, J., Cittadini, E., Peters, P., Scholberg, J., & Peri, P. (2012). Aeolian sediment mass fluxes on a sandy soil in Central Patagonia. *Catena*, *95*, 112–123. https://doi.org/10.1016/j.catena.2012.02.005
Vicari, A., Alexis, H., Del Negro, C., Coltelli, M., Marsella, M., & Proietti, C. (2007). Modeling of the 2001 lava flow at Etna volcano by a Cellular Automata approach. *Environmental Modelling and Software*, *22*(10), 1465–1471. https://doi.org/10.1016/j.envsoft.2006.10.005
Wang, G., Chen, J., Li, Q., & Ding, H. (2006). Quantitative assessment of land degradation factors based on remotely-sensed data and cellular automata: a case study of Beijing and its neighboring areas. *Environmental Sciences*, *3*(4), 239–253. https://doi.org/10.1080/15693430601063463
Webb, N. P., & McGowan, H. A. (2009). Approaches to modelling Land erodibility by wind. *Progress in Physical Geography*, *33*(5), 587–613. https://doi.org/10.1177/0309133309341604
Webb, N. P., Okin, G. S., & Brown, S. (2014). The effect of roughness elements on wind erosion: The importance of surface shear stress distribution. *Journal of Geophysical Research*, *119*(10), 6066–6084. https://doi.org/10.1002/2014JD021491
White, B. R. (1979). Soil Transport by Winds on Mars. *Journal of Geophysical Research*, *84*(B9), 4643–4651. https://doi.org/10.1029/jb084ib09p04643
Wolfe, S. A., & Nickling, W. G. (1993). The protective role of sparse vegetation in wind erosion. *Progress in Physical Geography*, *17*(1), 50–68. https://doi.org/10.1177/030913339301700104
Yousef, K. I., Abu-Awwad, A. M., & Rahbeh, M. (2018). The Effectiveness of Continuous Contour Ridges and Intermittent Trenches Constructed Using the Vallerani in Water Harvesting in Arid Regions. *Jordan Journal of Earth and Environmental Sciences*, *9*(3), 167–174. Retrieved from https://www.researchgate.net/publication/333812117
Zingg, A. W. (1953). Wind-Tunnel Studies of the Movement of Sedimentary Material. In *Proceedings of the Fifth Hydraulics Conference* (pp. 111–136).

Appendices

A Model results for 3 scenarios: bare conditions, water harvesting conditions without grass and water harvesting conditions with grass

B Model development with Okin (2008)

Appendix A

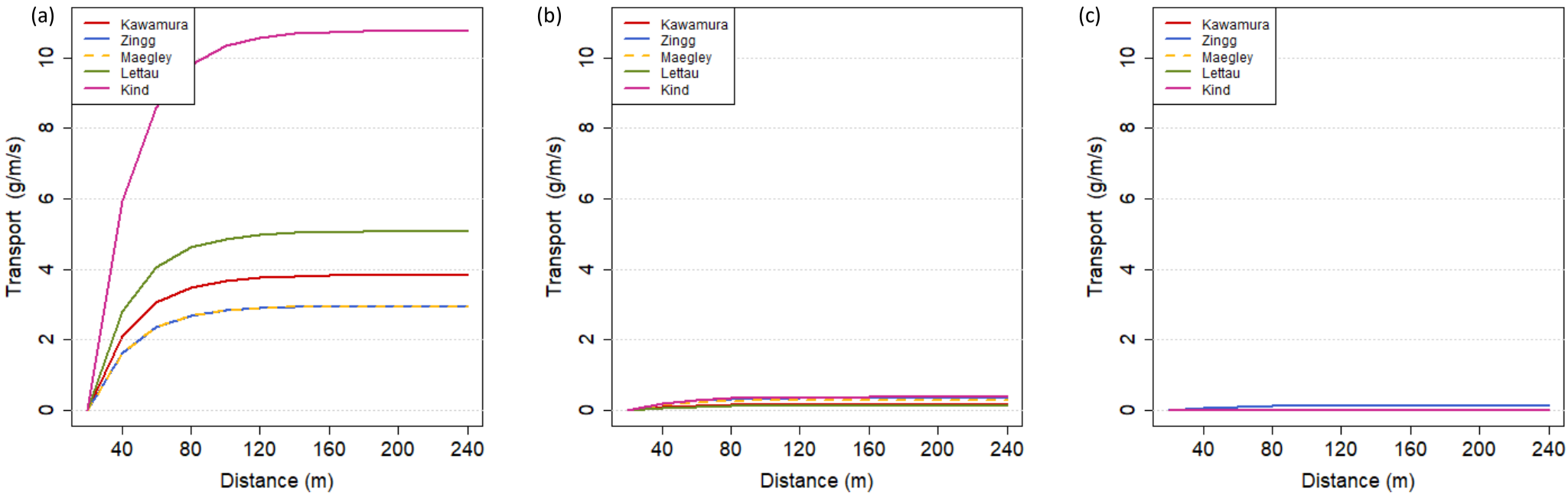

Figure A.1 Horizontal transport at the research site of all transport equations for a) bare conditions, b) water harvesting without grass conditions and c) water harvesting conditions with grass. Modelled for selected wind speed (14.89 m s-1 at 10m height) at 25-10-2018.

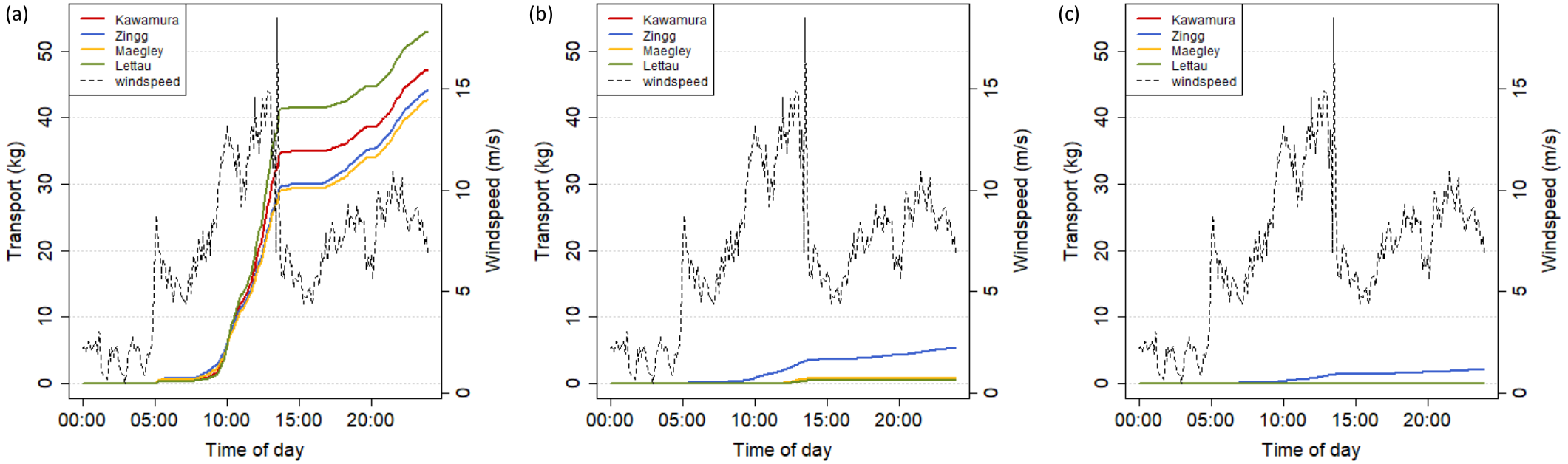

Figure A.2 Cumulative horizontal transport in last cell of the plot at the research site for selected transport equations for a) bare conditions, b) water harvesting without grass conditions and c) water harvesting conditions with grass over 24 hours on 25-10-2018.

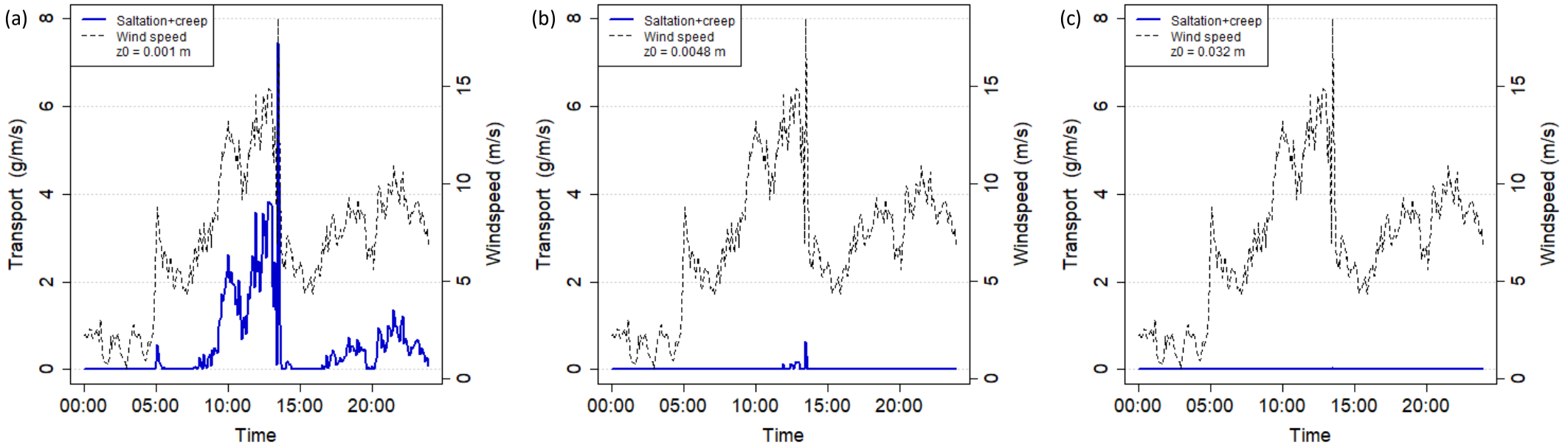

Figure A.3 Horizontal transport in last cell of the plot at the research site for Kawamura transport equations for a) bare conditions, b) water harvesting without grass conditions and c) water harvesting conditions with grass over 24 hours on 25-10-2018.

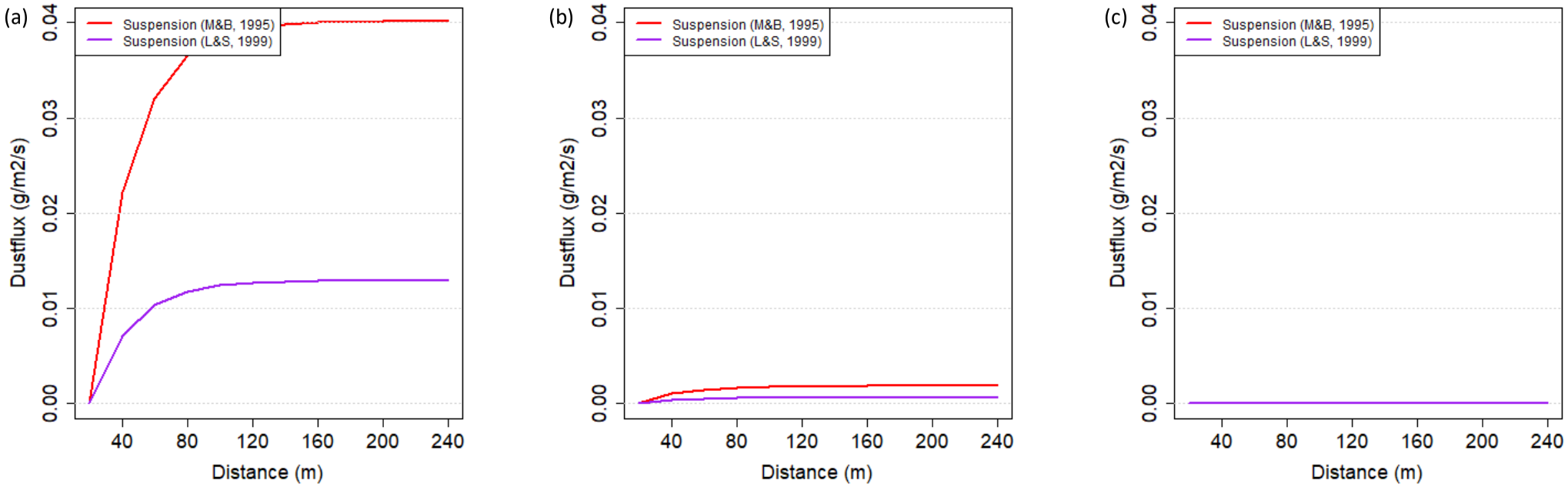

Figure A.4 Dust flux for 2 dust schemes at the research site for a) bare conditions, b) water harvesting without grass conditions and c) water harvesting conditions with grass. Modelled for selected wind speed (14.89 m s-1 at 10m height) at 25-10-2018.

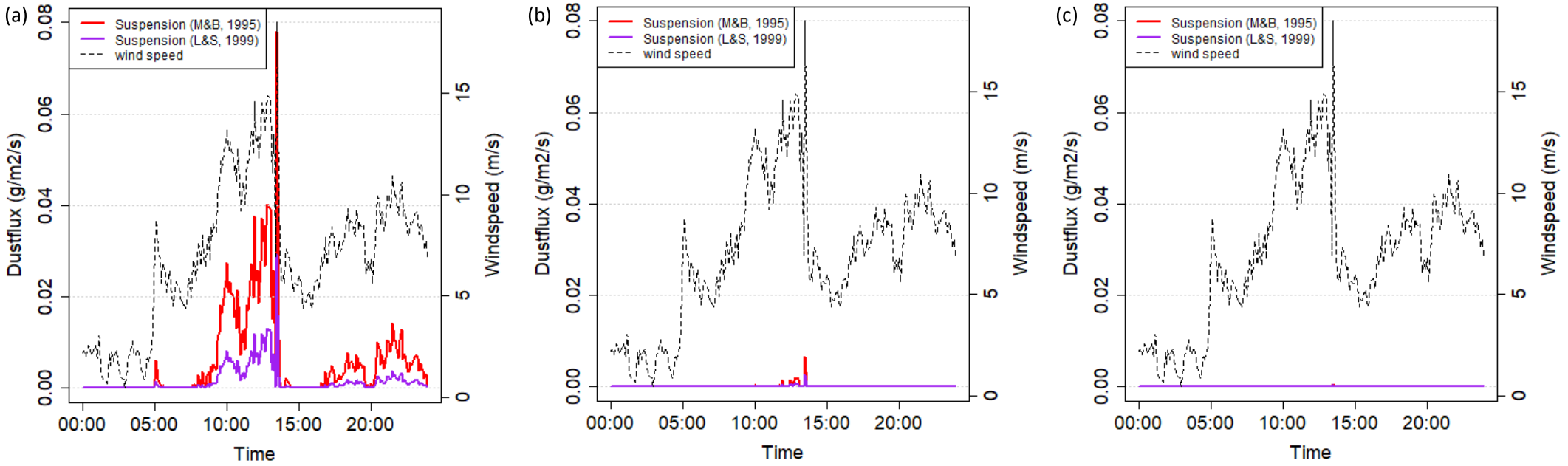

Figure A.5 Dust flux for 2 dust schemes in last cell of the plot at the research site for a) bare conditions, b) water harvesting without grass conditions and c) water harvesting conditions with grass over 24 hours on 25-10-2018.

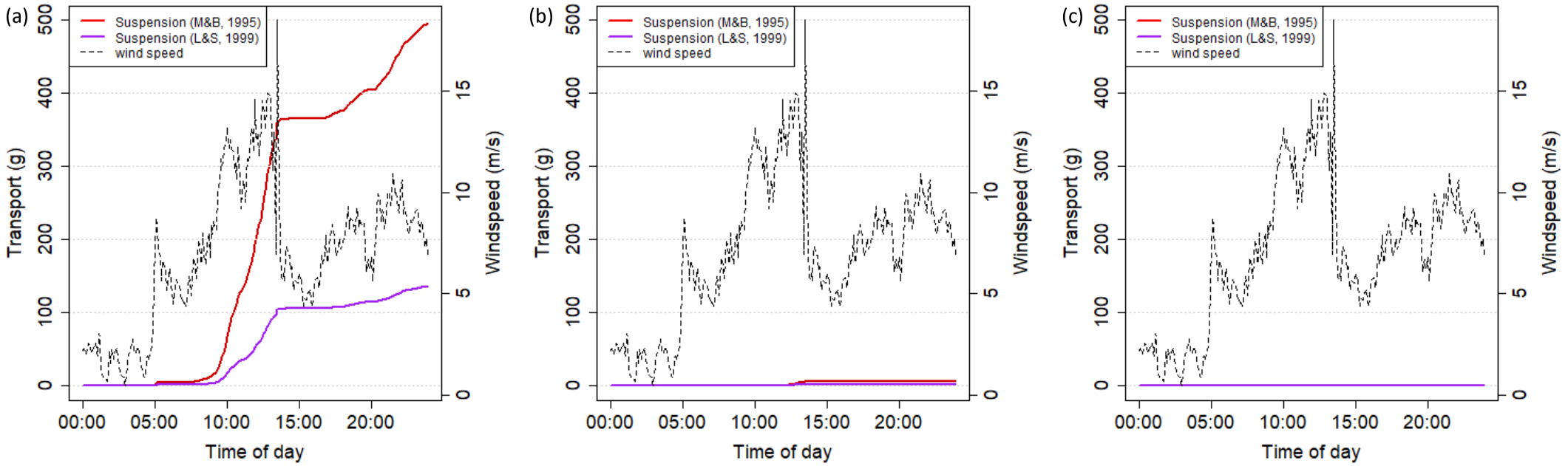

Figure A.6 Cumulative suspension for 2 dust schemes in last cell of the plot at the research site for a) bare conditions, b) water harvesting without grass conditions and c) water harvesting conditions with grass over 24 hours on 25-10-2018.

Appendix B

Model development with Okin (2008)

The CASS model from this research uses a cell size of 20 m, thereby averaging out vegetation values. This was done because the governing equations were developed for such distances, and reducing the cell size without field validation was deemed inaccurate. However, an improved model set-up has been created that uses a cell size of 1 m, that can be used if necessary parameters can be validated with field measurement. The general model set-up is the same as described in Chapter 3, with some alterations when it comes to the drag partitioning and vegetation settings. Here, an initial overview is given.

Okin (2008) attempted to incorporate the effect of the heterogeneity of the vegetation by adding a gap size parameter representative for the spatial distribution. The gap size creates a zone of reduced friction velocity behind the roughness element, the so called wake zone (Wolfe & Nickling, 1993). They use an exponential curve to alter the friction velocity on the surface behind the plant based on the distance towards the nearest upwind plant:

$$u_{*s} = u_* * \left(\left(\frac{u_{*s}}{u_*} \right) + \left(1 - \left(\frac{u_{*s}}{u_*} \right) \right) * \left(1 - \exp\left(\frac{d_p}{\frac{1}{2} b_{sh}} \right) \right) \right) \quad (A.1)$$

where d_p is the distance to the nearest upwind plant. This equation was implemented in the improved model, as the cell size allowed the distinction of such a wake-zone (which could not be done in the original CASS model).

As the horizontal sediment flux is based on the maximum horizontal sediment flux, the model uses an additional function to estimate the maximum horizontal flux in the vegetated zones, assuming that this maximum flux is strongly reduced but not zero in those zones. Although all transport equations used in the original model (*3.16-3.18*) can be applied, the improved model has only been run with the Kawamura equation (1964).

Two vegetation scenarios are initially implemented in the model: bare soil and water harvesting without grass (Figure A.7). These were chosen as the incorporation of grasses is still complex, but can be expanded in further studies.

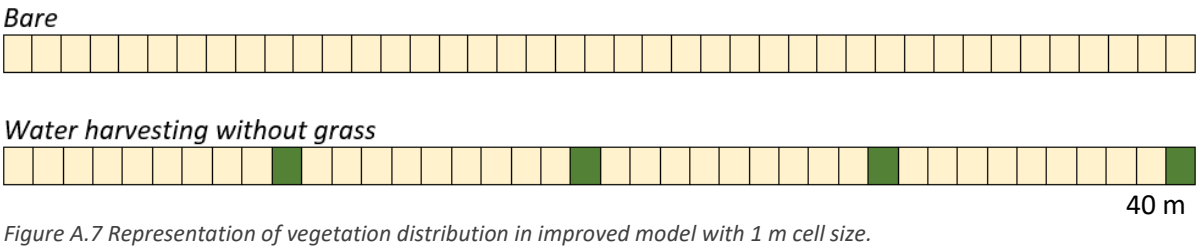

Figure A.7 Representation of vegetation distribution in improved model with 1 m cell size.

The main difference in results of the improved model is the horizontal transport graph (Figure A.8). The development of the flux for the bare conditions is equal to the original model results (Figure 15a). For the water harvesting conditions, there is now clearly a spatial pattern visible, indicating the position of the water harvesting rows and the resulting reduction of transport both at and just behind these shrubs. The same effect can be seen in in the vertical dust flux for the 2 dust schemes incorporated in the model (Figure A.9).

These new patterns seem intuitively more correct than the results from the original, as the effect of the water harvesting structures is that they trap sediment, but between the rows the flux can develop with the wind. However, it should be noted that it is unclear if the model equations can be

applied on such a small scale (1 m grid size). Field measurements are therefore needed to validate these values and possibly incorporate a correction factor. Further research is also needed to assess total transport reductions and the applicability of this approach for dust modelling.

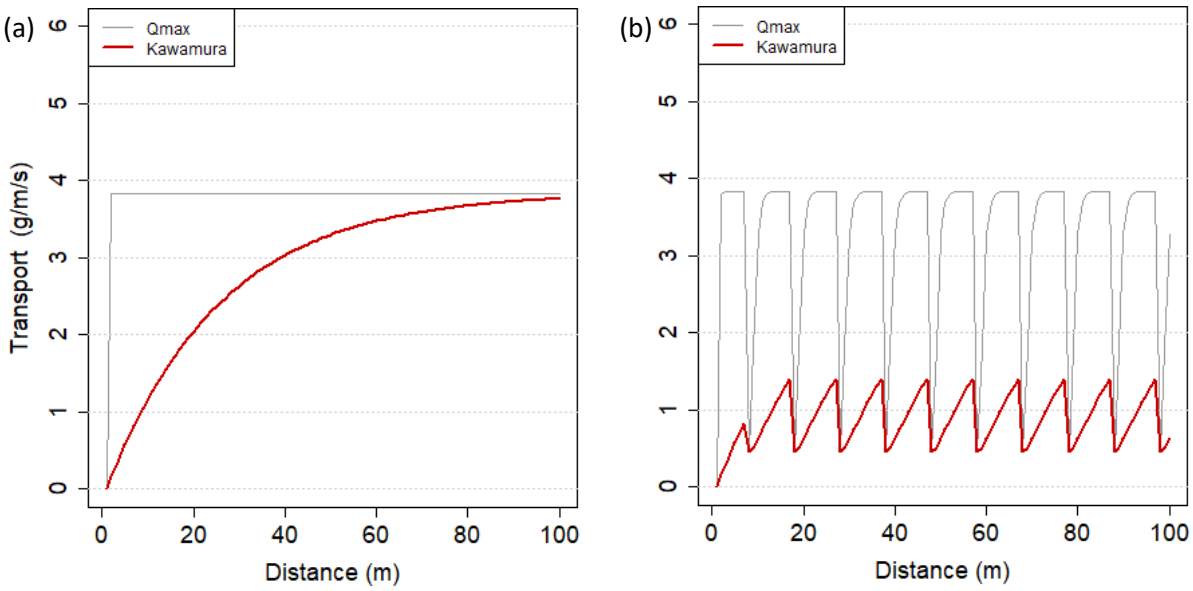

Figure A.8 Horizontal transport at the research site for the Kawamura (1964) equation for a) bare conditions and b) water harvesting without grass conditions. Modelled for selected wind speed (14.89 m s^{-1} at 10m height) at 25-10-2018, following the approach of Okin (2008).

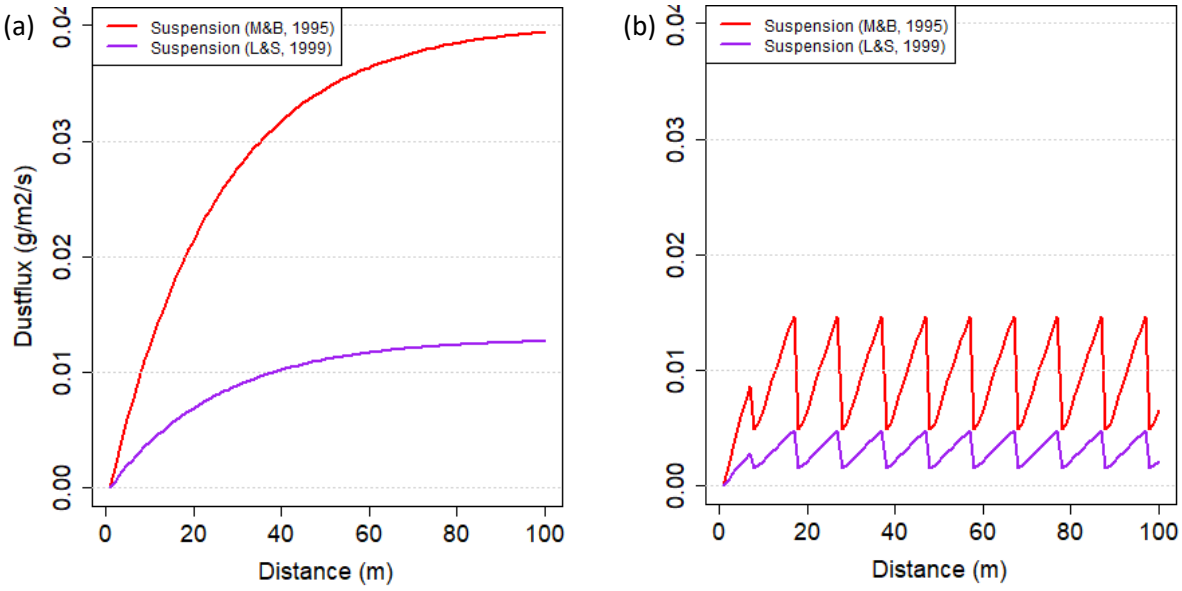

Figure A.9 Vertical dust flux for 2 dust schemes at the research site for a) bare conditions and b) water harvesting without grass conditions. Modelled for selected wind speed (14.89 m s^{-1} at 10m height) at 25-10-2018. following the approach of Okin (2008).